Low-lying magnetic excitations in amorphous $Fe_{90-x}Co_xZr_{10}$ and $Fe_{90+y}Zr_{10-y}$ alloys

1998 J. Phys.: Condens. Matter 10 1563

(http://iopscience.iop.org/0953-8984/10/7/009)

J. Phys.: Condens. Matter **10** (1998) 1563–1597. Printed in the UK PII: S0953-8984(98)88260-X

Low-lying magnetic excitations in amorphous $Fe_{90-x}Co_xZr_{10}$ and $Fe_{90+y}Zr_{10-y}$ alloys

S N Kaul† and P D Babu‡

School of Physics, University of Hyderabad, Central University PO, Hyderabad 500 046, Andhra Pradesh, India

Received 7 October 1997

Abstract. Results of high-resolution magnetization (M) measurements performed on amorphous (a-) $Fe_{90-x}Co_xZr_{10}$ ($x = 0, 1, 2, 4, 6, 8, 10$) and $Fe_{90+y}Zr_{10-y}$ ($y = 0, 1$) alloys over wide ranges of temperature (T) and external magnetic field (H_{ext}) are presented and discussed in the light of existing theoretical models. The magnetization at 5 K does not saturate even for fields as high as 70 kOe particularly for the alloys with $x \lesssim 6$ and $y = 0, 1$. The high-field differential susceptibility at $T = 5$ K, $\chi_{hf}(0)$, is extremely large for the alloys with $x = 0, 1$ and $y = 0, 1$, and decreases rapidly with x for $x \lesssim 4$ such that it possesses values typical of crystalline ferromagnets such as Fe, Co, Ni for $x > 6$. The dominant contribution to the thermal demagnetization of the spontaneous as well as 'in-field' magnetization comes from spin-wave (SW) excitations at low temperatures ($T \lesssim 0.4T_C$) and from enhanced local spin-density fluctuations over a wide range of intermediate temperatures ($0.45T_C \lesssim T \lesssim 0.75T_C$) and for temperatures close to the Curie point, T_C ($0.7T_C \lesssim T \lesssim 0.95T_C$), for all of the alloys studied. The spin-wave stiffness, D, is *independent* of H_{ext} for all of the compositions and the D/T_C ratio possesses a value $\approx$0.14 *characteristic* of amorphous ferromagnets with *competing* interactions for the alloys with $x \lesssim 6$ and $y = 0, 1$. For these alloys, thermomagnetic and thermoremanent effects generally associated with the cluster spin-glass behaviour have been observed in the re-entrant state which sets in at a temperature T_{RE}. In accordance with the predictions of the spin-fluctuation model, D renormalizes with temperature as $D(T) = D(0)(1 - D_2T^2)$ and the spin fluctuations get strongly suppressed by Co substitution and H_{ext}. While the spin-fluctuation (SF) model provides a consistent theoretical basis for the observed temperature dependence of the spontaneous and 'in-field' magnetization over the entire temperature range $0 \lesssim T \lesssim T_C$, the infinite three-dimensional (FM) matrix plus finite FM spin-clusters model extends the scope of the SF model in that it offers a straightforward explanation for the absence of SW peaks in the inelastic neutron scattering spectra taken over a certain wave-vector-transfer range, the softening of spin-wave modes for $T < T_{RE}$, the existence of a significant contribution due to diffusons, in addition to magnons, to the $T^{3/2}$-decrease of the magnetization, and the composition dependence of $D(0)$, $M(0, 0)$ and T_C.

1. Introduction

Amorphous (a-) $Fe_{90+y}Zr_{10-y}$ ($0 \leqslant y \leqslant 3$) and $Fe_{90-x}(Co, Ni)_xZr_{10}$ alloys figure among the most extensively studied amorphous magnetic systems, and yet several aspects of their magnetism have eluded a complete understanding so far. One such aspect pertains to the existence of well-defined spin-wave excitations in the former system. While the

† Author to whom any correspondence should be addressed.

‡ Present address: Inter University Consortium for DAE Facilities, Bombay Centre, Bhabha Atomic Research Centre, Trombay, Bombay-400 085, India.

0953-8984/98/071563+35$19.50

bulk magnetization (BM) data [1–3] taken on a-$Fe_{90+y}Zr_{10-y}$ ($y = 0$, 1) alloys clearly demonstrate that the temperature dependence of both the spontaneous magnetization, $M(T, 0)$, and the 'in-field' magnetization, $M(T, H)$, is mainly governed by spin-wave excitations at temperatures $T \lesssim 0.4T_C$, constant-q scans taken for the wave-vector-transfer range 0.05 $\text{Å}^{-1} \leqslant q \leqslant 0.12$ Å^{-1} in inelastic neutron scattering (INS) experiments [4] on a-$Fe_{91}Zr_9$ show no evidence of propagating spin waves at any temperature $T < T_C$ (T_C is the Curie temperature). However, when only about 1 at.% Fe in a-$Fe_{90}Zr_{10}$ host is replaced by Ni, well-defined spin-wave peaks [5] are observed in the INS constant-q scans taken for wave vectors 0.04 $\text{Å}^{-1} \leqslant q \leqslant 0.10$ Å^{-1} at temperatures $0.2T_C \leqslant T \leqslant 0.91T_C$. Moreover, the values, D_M, of the spin-wave stiffness, D, estimated from the BM data [6] for the alloys with $x = 5$, 10 and 20 in the series a-$Fe_{90-x}Ni_xZr_{10}$ are consistently *lower* than those, D_N, measured in the INS experiments, and the D_N/D_M ratio increases from $\approx$1.1 at $x = 5$ to $\approx$1.6 at $x = 20$. Considering that D possesses a value [2] ($D_M = 29 \pm 1$ meV Å^2 for a-$Fe_{91}Zr_9$) which lies well above the resolution limit $D_N \approx 15$ meV Å^2 of the INS measurements [4] on a-$Fe_{91}Zr_9$ and that D_N is expected to equal, if not greatly exceed, D_M, a total absence of the attributes of spin waves in the INS spectra taken on a-$Fe_{91}Zr_9$ is incomprehensible. Equally inexplicable is the extreme sensitivity of spin waves to Ni substitution. With a view to arriving at a basic understanding of these observations, a systematic study of the modification in the spin-wave behaviour as x is increased from 0 to 10 at.% in the a-$Fe_{90-x}Co_xZr_{10}$ alloy series was undertaken. The rationale behind the choice of this system is that partial replacement of Fe by Co alters the magnetic properties such as the value of T_C, the magnetic moment at 0 K, the Invar characteristics and the re-entrant behaviour at low temperatures of the a-$Fe_{90}Zr_{10}$ host in the *same* way as [7, 8] (but more drastically by comparison than) Ni substitution does.

By revealing that (i) local spin-density fluctuations (LSF) contribute dominantly to the thermal demagnetization of $M(T, 0)$ for a-$Fe_{90+y}Zr_{10-y}$ ($y = 0, 1$) alloys over a wide range of intermediate temperatures and for $T \approx T_C$ while Stoner single-particle (SP) excitations are mainly responsible for the decline of $M(T, 0)$ with increasing temperature for $T \gtrsim 0.1T_C$ for a-$Co_{90}Zr_{10}$, and (ii) an external magnetic field of strength $H_{ext} = 15$ kOe strongly suppresses LSF in the former set of alloys but has no discernible effect on $M(T)$ for a-$Co_{90}Zr_{10}$, BM measurements [1–3, 9] on a-$Fe_{90+y}Zr_{10-y}$ ($y = 0$, 1) and a-$Co_{90}Zr_{10}$ alloys have raised the following basic questions. (a) Does the insensitivity of $M(T)$ to H_{ext} in a-$Co_{90}Zr_{10}$ imply the complete absence of LSF in this system? (b) If so, why are LSF absent in a-$Co_{90}Zr_{10}$? (c) Can the suppression of LSF by H_{ext} be quantified? In order to seek answers to these questions, a detailed investigation of the magnetization as a function of temperature and external magnetic field, H_{ext}, for a-$Fe_{90-x}Co_xZr_{10}$ and a-$Fe_{90+y}Zr_{10-y}$ alloys is called for. Considering the fact that LSF are present in a-$Fe_{90}Zr_{10}$ but could be absent in a-$Co_{90}Zr_{10}$, such an investigation is expected to bring out clearly the roles played by Co substitution and H_{ext} in suppressing LSF. In this context, it is interesting to note that the existence of LSF in a-$Fe_{90+y}Zr_{10-y}$ alloys has also been recently inferred from the electrical resistivity data [10].

2. Theoretical background

In this section, we furnish the relevant details about the spin-fluctuation (SF) model, which, as we shall show later, puts most of our observations on a consistent theoretical footing. This model makes use of the Ginzburg–Landau (GL) expansion of the *local* free-energy density in terms of a small slowly varying *classical* order parameter (the local magnetization)

$\boldsymbol{M} + m(\boldsymbol{r})$ and yields the magnetic equation of state in the form [11]

$$H/M(T, H) = a(T) + b(3\langle m_{\parallel}^2\rangle + 2\langle m_{\perp}^2\rangle) + bM^2(T, H) \tag{1}$$

with

$$\langle m_{\nu}^2\rangle = 4\hbar \int \frac{\mathrm{d}^3\boldsymbol{q}}{(2\pi)^3} \int_0^{\infty} \frac{\mathrm{d}\omega}{2\pi}\, n(\omega)\, \mathrm{Im}\, \chi_{\nu}(\boldsymbol{q}, \omega) \tag{2}$$

$$n(\omega) = [\exp(\hbar\omega/k_BT) - 1]^{-1} \tag{3}$$

$$a(T) = -[2\chi(0, 0)]^{-1}[1 - (T/T_C^S)^2 - \mathcal{B}\mathcal{S}T^4] \tag{4}$$

$$b(T) = [2\chi(0, 0)M^2(0, 0)]^{-1} \tag{5}$$

$$\chi(0, 0) = N\mu_B^2 N(E_F)(T_F/T_C^S)^2 = N\mu_B^2 N(E_F)\mathcal{S} \tag{6}$$

$$M^2(0, 0) = (N\mu_B\mu_0)^2 = (\mathcal{S}\gamma)^{-1} \tag{7}$$

$$T_F^{-2} = (\pi^2 k_B^2/6)\nu' \tag{8}$$

$$\nu' = [N'(E_F)/N(E_F)]^2 - [N''(E_F)/N(E_F)] \tag{9}$$

$$\mathcal{S} = [IN(E_F) - 1]^{-1} \tag{10}$$

$$\gamma = \{8N^2\mu_B^2 N^2(E_F)\}^{-1}\{[N'(E_F)/N(E_F)]^2 - [N''(E_F)/3N(E_F)]\}. \tag{11}$$

In the above equations, $\langle m_{\parallel}^2\rangle$ and $\langle m_{\perp}^2\rangle$ are the thermal variances of the local magnetization parallel ($\parallel$) and perpendicular ($\perp$) to the average magnetization $\boldsymbol{M}$, respectively, ν ($= \parallel$, $\perp$) is the polarization index, $n(\omega)$ is the Bose function, $\chi_{\nu}(\boldsymbol{q}, \omega)$ is the dynamical wave-vector-dependent susceptibility, a and b are the Landau coefficients for the Stoner theory [12], $\chi(0, 0)$ and μ_0 are the zero-field differential susceptibility and magnetic moment per alloy atom at 0 K, $\mathcal{S}$ is the Stoner enhancement factor, I (the Stoner parameter) is a measure of the exchange splitting of the bands, N is the number of atoms per unit volume, $N(E_F)$ is the density of single-particle states (DOS) at the Fermi level E_F and $N'(E_F)$ ($N''(E_F)$) is its first (second) energy derivative, T_C^S is the Stoner Curie temperature and the coefficient $\mathcal{B}$ of the T^4-term in equation (4) involves derivatives of the DOS at E_F up to fourth order and its explicit form is given in reference [13]. In the absence of an external magnetic field, equations (1)–(11) permit calculation of $M(T, 0)$ for $T < T_C$ as follows. When $H = 0$, equation (1) reduces to

$$M^2(T, 0) = -(a(T)/b) - (3\langle m_{\parallel}^2\rangle + 2\langle m_{\perp}^2\rangle). \tag{12}$$

Equations (4), (5) and (12), when combined, yield

$$[M(T, 0)/M(0, 0)]^2 = 1 - (T/T_C^S)^2 - \mathcal{B}\mathcal{S}T^4 - (3\langle m_{\parallel}^2\rangle + 2\langle m_{\perp}^2\rangle)/M^2(0, 0). \tag{13}$$

The exact functional form of $M(T, 0)$ in different temperature ranges below T_C can be derived from equation (13) with the aid of equation (2) provided that it is recognized that $\langle m_{\nu}^2\rangle$ consists of two parts: a spin-wave (SW) part, which is dominant at low temperatures, and a SF part which dominates at intermediate temperatures and for temperatures close to T_C. The contributions to the thermal demagnetization of $M(T, 0)$ due to the $\langle m_{\nu}^2\rangle_{SW}$ and $\langle m_{\nu}^2\rangle_{SF}$ components are obtained from equation (2) by inserting the following expressions [11] for $\mathrm{Im}\, \chi_{\nu}(\boldsymbol{q}, \omega)$ in this equation and then evaluating the integrals:

$$[\mathrm{Im}\, \chi_{\perp}(\boldsymbol{q}, \omega)]_{SW} = \frac{\pi}{2}\omega\chi_{\perp}(\boldsymbol{q})[\delta(\omega - \omega(\boldsymbol{q})) + \delta(\omega + \omega(\boldsymbol{q}))] \tag{14}$$

and

$$[\mathrm{Im}\, \chi_{\nu}(\boldsymbol{q}, \omega)]_{SF} = \omega\chi_{\nu}(\boldsymbol{q})\frac{\Gamma_{\nu}(\boldsymbol{q})}{\omega^2 + \Gamma_{\nu}^2(\boldsymbol{q})} \tag{15}$$

with the spin-wave propagation frequency $\omega(\boldsymbol{q})$ and the *relaxation* frequency of a spontaneous spin fluctuation of wave vector $\boldsymbol{q}$ and polarization ν (one parallel and two perpendicular to $\boldsymbol{M}$) $\Gamma_\nu(\boldsymbol{q})$ given by [11]

$$\hbar\omega(\boldsymbol{q}) = g\mu_B M(T,H)\chi_\perp^{-1}(\boldsymbol{q}) = g\mu_B M(T,H)(\chi_\perp^{-1} + c_\perp q^2 + \cdots) \tag{16}$$

and

$$\Gamma_\nu(\boldsymbol{q}) = \gamma_\nu' q\chi_\nu^{-1}(\boldsymbol{q}) = \gamma_\nu' q(\chi_\nu^{-1} + c_\nu q^2 + \cdots) \tag{17}$$

respectively, in the random-phase approximation (RPA) at low q and for a cubic lattice. In equations (16) and (17), $\chi_\nu(\boldsymbol{q}) = \chi_\nu(\boldsymbol{q}, \omega = 0)$ is a component of the static susceptibility, $\chi_\nu = \chi_\nu(\boldsymbol{q} = 0)$, and g is the Landé splitting factor, while the parameters $\gamma' = (4/\pi)\mathcal{S}^{-1}\chi(0,0)v_F + \cdots$ (to zeroth order in $\langle m^2\rangle$, where v_F is the Fermi velocity) and c (the coefficient of the gradient term in the Ginzburg–Landau expansion) are *independent* of ν for small M.

At low temperatures ($T < 0.3T_C$), $T \ll T_C^S$ and the term $\mathcal{B}\mathcal{S}T^4$ in equation (13) is negligibly small, so equation (13) can be approximated by

$$\frac{M(T,0)}{M(0,0)} \simeq 1 - \frac{\langle m_\perp^2\rangle}{M^2(0,0)} - \frac{3}{2}\frac{\langle m_\parallel^2\rangle}{M^2(0,0)}. \tag{18}$$

The thermal demagnetization of $M(T,0)$ in crystalline (homogeneous) ferromagnets at low temperatures is mainly due to spin-wave excitations (*propagating* transverse spin fluctuations), i.e., the second term in equation (18) is very large compared to the third. Equation (14), when it is substituted in equation (2) and the result inserted in equation (18), yields the well-known Bloch $T^{3/2}$ power law

$$\frac{M(T,0)}{M(0,0)} = 1 - \frac{g\mu_B}{M(0,0)}\xi(3/2)\left[\frac{k_BT}{4\pi D(T)}\right]^{3/2} \tag{19}$$

where $\xi(3/2)$ is the Riemann zeta function. Equation (16) relates the spin-wave stiffness, $D(T)$, to $M(T,0)$ via the expression $D(T) = g\mu_B c_\perp M(T,0)$ and, considering that $\chi_\perp^{-1} = \partial H_\perp/\partial M_\perp = H/M$, gives the spin-wave energy gap equal to $g\mu_B H$ when $H \neq 0$. Note that H stands for the *effective* field $H_{eff} = H_{ext} - 4\pi N M(T, H_{ext}) + H_A$, where N is the demagnetizing factor and H_A is the anisotropy field (corresponding to the forms of anisotropy, other than the shape anisotropy, that are present in the system under consideration). In the presence of H_{ext}, equation (19) takes the form

$$\frac{M(T,H)}{M(0,H)} = 1 - \frac{g\mu_B}{M(0,H)}Z(3/2,t_H)\left[\frac{k_BT}{4\pi D(T)}\right]^{3/2} \tag{20}$$

where the Bose–Einstein integral function

$$Z(3/2,t_H) = \xi(3/2)F(3/2,t_H) = \sum_{n=1}^{\infty} n^{-3/2}\mathrm{e}^{-nt_H}$$

with $t_H = T_g/T = g\mu_B H/k_BT$ allows for the energy gap in the spin-wave spectrum. In the case of crystalline or amorphous ferromagnets with competing interactions and/or Invar characteristics, the contribution to $M(T,0)$ arising from longitudinal spin fluctuations, i.e., from the third term in equation (18), cannot be ignored even at low temperatures since the orientation of a given magnetic moment in such systems is, in general, not parallel to the direction of bulk magnetization. As a consequence, the displacements of the longitudinal component of the magnetization from the local equilibrium value are of the same order of magnitude as the transverse displacements which give rise to spin waves. Thus, the diffusive modes ('diffusons') associated with the longitudinal component of the magnetization (which

are of hydrodynamic origin) contribute to the $T^{3/2}$-decrease of magnetization as significantly as the transverse fluctuations (spin waves) do. In sharp contrast with spin waves (*undamped* modes), diffusons represent *overdamped* modes that are described by equation (2) with $\mathrm{Im}\,\chi_\parallel(\boldsymbol{q},\omega)$ given by the version of equation (15) in which [14] $\Gamma_\parallel(\boldsymbol{q}) = D_i q^2$ and D_i is the diffusion constant. The contribution due to diffusons to $M(T,0)$, computed from equation (2) and the modified version of equation (15), is given by [14]

$$\langle m_\parallel^2\rangle = \frac{\mathcal{A}}{2}\xi(3/2)\left(\frac{k_B T}{2\pi D_i}\right)^{3/2} \tag{21}$$

where $\mathcal{A}$ is a constant. According to equations (18), (19) and (21), thermal demagnetization of $M(T,0)$ is *faster* in spin systems in which diffusons, in addition to spin waves, do contribute to the $T^{3/2}$-dependence of $M(T,0)$. However, unlike magnons, diffusons show up as a broad central (elastic) peak [14] in the inelastic neutron scattering intensity versus neutron energy isotherms taken at constant values of q (i.e., in the INS constant-q scans). An immediate consequence of this prediction is that the value of D deduced from the magnetization data, D_M, should be substantially *lower* than that measured in the INS experiments, D_N, in such systems. Such a discrepancy between the values of D, i.e., $D_N \gg D_M$, has indeed been found for a number of Invar systems.

In the intermediate range of temperatures (typically, $0.4T_C < T < 0.8T_C$), the spin-wave contribution to $M(T,0)$ is completely swamped by the SF contribution, which, in this temperature range, varies with T as [11]

$$\frac{\langle m_v^2\rangle_{SF}}{M^2(0,0)} = \frac{(3\langle m_\parallel^2\rangle + 2\langle m_\perp^2\rangle)_{SF}}{M^2(0,0)} = \left(\frac{T}{T_0}\right)^2. \tag{22}$$

Combining equations (13) and (22), one obtains

$$\left[\frac{M(T,0)}{M(0,0)}\right]^2 = 1 - \left[\left(\frac{1}{T_C^S}\right)^2 + \left(\frac{1}{T_0}\right)^2\right]T^2 - \mathcal{BS}T^4 = 1 - \left(\frac{T}{T_C^*}\right)^2 + \mathcal{B}'T^4 \tag{23}$$

where $(1/T_C^*)^2 = (1/T_C^S)^2 + (1/T_0)^2$ and $\mathcal{B}' = -\mathcal{BS}$. The last term in equation (23) is normally too small to merit consideration because the coefficient $\mathcal{B}$ usually has a value close to zero (note that depending upon the structure of the DOS curve and hence on the relative magnitude of its derivatives, $\mathcal{B}$ can be either positive, negative or zero) but it can be *significant* for systems in which $\mathcal{S}$ has an *extremely large* value, i.e., for very weak itinerant ferromagnets in which $IN(E_F) \to 1$ and hence $\mathcal{S} \to \infty$. From the coefficient of the T^2-term in equation (23), it is evident that LSF (Stoner SP excitations) dominantly contribute to $M(T,0)$ if $T_0 \ll T_C^S$ ($T_C^S \ll T_0$). However, if $T_0 \approx T_C^S$, the contributions due to LSF and SP excitations are comparable in magnitude. Recognizing that equation (23) can be put into the form $[M(T,0)/M(0,0)]^2 = 1 - 2AT^2 + A^2T^4$, equation (23) can be generalized to

$$M(T,H)/M(0,H) = 1 - A(H)T^2 \tag{24}$$

or

$$[M(T,H)/M(0,H)]^2 = 1 - 2A(H)T^2 \equiv 1 - A''(H)T^2 \tag{25}$$

depending upon whether the T^4-term is of significant magnitude or is negligibly small compared to the T^2-term. Equations (24) and (25) are valid for the situations in which H is either finite or zero. When $H = 0$, the value of the *effective* Curie temperature can be obtained from the relation $T_C^{eff} = 1/\sqrt{A(0)}$ (equation (24)) or $T_C^{eff} = 1/\sqrt{2A(0)} = 1/\sqrt{A''(0)}$ (equation (25)) as the case may be.

For temperatures close to T_C ($0.8T_C < T < 0.95T_C$), $\chi_{\parallel}^{-1} \approx \chi_{\perp}^{-1}$ and the longitudinal and transverse fluctuations are thus treated on the same footing with the result that the temperature variation of the LSF contribution is accurately given by [11]

$$\frac{(3\langle m_{\parallel}^2\rangle + 2\langle m_{\perp}^2\rangle)_{SF}}{M^2(0,0)} = \left(\frac{T}{T_1}\right)^{4/3} \tag{26}$$

where

$$T_1 = 2.387D(0)\sqrt{M(0,0)}(\hbar\gamma')^{1/4}/g\mu_B k_B.$$

At such temperatures, the spin splitting of the bands is approaching zero, $N(E_F)$ and its derivatives are undergoing substantial changes especially for weak itinerant ferromagnets (for which the T^4-term in equation (13) is of significant magnitude at intermediate temperatures) and, consequently, the coefficient $\mathcal{B}$ assumes a considerably reduced value compared to that in the intermediate-temperature range. Substituting equation (26) for the SF term and completely dropping the T^4-term in equation (13) gives

$$\left[\frac{M(T,0)}{M(0,0)}\right]^2 = 1 - \left(\frac{T}{T_C^S}\right)^2 - \left(\frac{T}{T_1}\right)^{4/3}. \tag{27}$$

The Curie temperature T_C can be determined from equation (27) using the condition $M(T,0) = 0$ at $T = T_C$ provided that the values of T_C^S and T_1 are known. Alternatively, at $T = T_C$, equation (27) has the form

$$1 - \left(\frac{T_C}{T_C^S}\right)^2 - \left(\frac{T_C}{T_1}\right)^{4/3} = 0. \tag{28}$$

From equation (28), it follows that $T_C = T_C^S$ if $T_C^S \ll T_1$ and $T_C = T_1$ if $T_1 \ll T_C^S$. In these two extreme limits, SP excitations and enhanced LSF are respectively predominant. Specifically in the latter limit, equation (27) reduces to

$$\left[\frac{M(T,0)}{M(0,0)}\right]^2 = 1 - \left(\frac{T}{T_C}\right)^{4/3}. \tag{29}$$

In analogy with equation (23), in the presence of H, equation (29) can be generalized to

$$\left[\frac{M(T,H)}{M(0,H)}\right]^2 = 1 - A'(H)T^{4/3} \tag{30}$$

so $A'(H=0) \equiv A'(0) = T_C^{-4/3}$.

3. Experimental details

Magnetization versus H_{ext} isotherms in fields up to 15 kOe for amorphous (a-) $Fe_{90-x}Co_xZr_{10}$ alloys with $x = 0$, 1, 2, 4, 6 and a-$Fe_{90+y}Zr_{10-y}$ alloys with $y = 0$, 1 were measured at temperatures ~1 K and ~0.15 K apart in the ranges 68 K $\leqslant T \lesssim T_C - 15$ K and $T_C - 15$ K $\lesssim T \lesssim T_C$, respectively, on an EG&G Princeton Applied Research Vibrating Sample Magnetometer (VSM) 4500 system, and M–H_{ext} isotherms in fields up to 70 kOe for a-$Fe_{90-x}Co_xZr_{10}$ alloys with $x = 0, 1, 2, 4, 6, 8, 10$ and a-$Fe_{90+y}Zr_{10-y}$ alloys with $y = 0, 1$ was measured at $T = 5$ K on a Quantum Design SQUID Magnetometer MPMS7. Each isotherm (the isotherm at 5 K) was obtained by measuring the magnetization at 55 (180) predetermined fixed field values in the range $0 \leqslant H_{ext} \leqslant 15$ kOe ($0 \leqslant H_{ext} \leqslant 70$ kOe). The temperature stability was better than ±25 mK and ±40 mK for the VSM

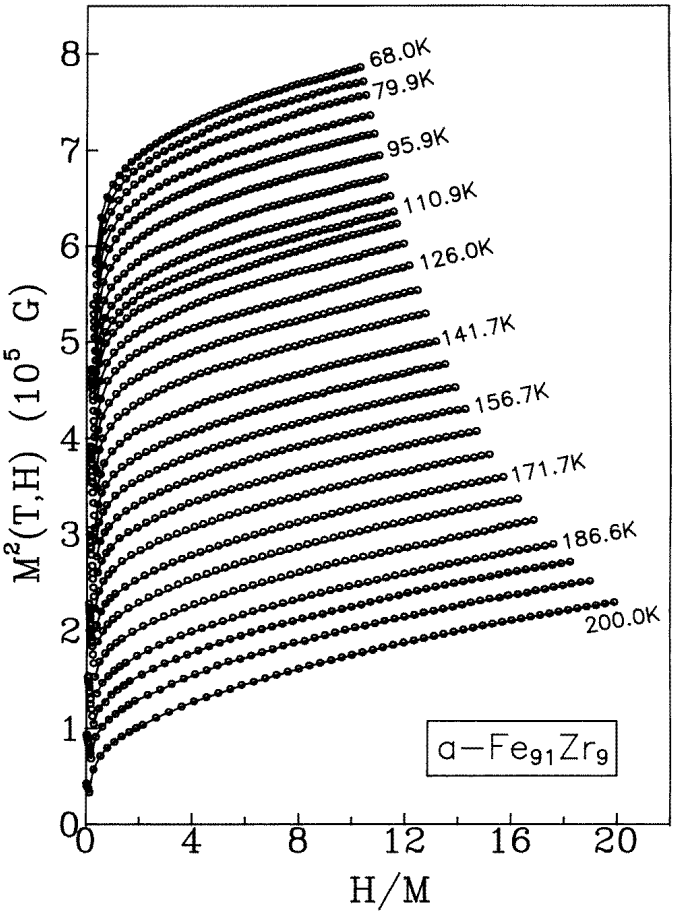

Figure 1. M^2 versus H/M isotherms at a few representative temperatures for a-$Fe_{91}Zr_9$. Here $H \equiv H_{eff}$.

isotherms at $T \leqslant 300$ K and $T > 300$ K (± 10 mK for the SQUID isotherm). The magnetization measurements made using the VSM were extended to temperatures beyond 300 K only for the alloys with $x = 4$ and 6 since their Curie temperatures exceed the room temperature. Since $T_C = 375$ K and (the crystallization temperature) $T_{cr} \approx 750$ K for the alloy with $x = 6$, the sample with this composition, before proceeding with the above measurements, was annealed at 450 K for different durations of time until no shift in T_C was observed in the 'kink-point' measurements [15]. The bulk magnetization was also measured as a function of temperature at $H_{ext} = 10$ kOe (various constant applied magnetic field values in the low-field region, i.e., 10 Oe $\lesssim H_{ext} \lesssim$ 500 Oe), for all of the samples (for all of the samples except the ones with $x = 8$ and 10) mentioned above in the heating cycle only (in both heating and cooling cycles) at $\sim$1 K intervals in the temperature range 5 K $\leqslant T \leqslant$ 350 K using the SQUID magnetometer. Relevant details concerning the sample preparation and characterization are given in our earlier reports [1–3, 9, 16].

The M versus H_{ext} isotherms were converted into a form that gives the magnetization as a function of the temperature at fixed values of H_{ext}, 1 kOe apart, in the interval

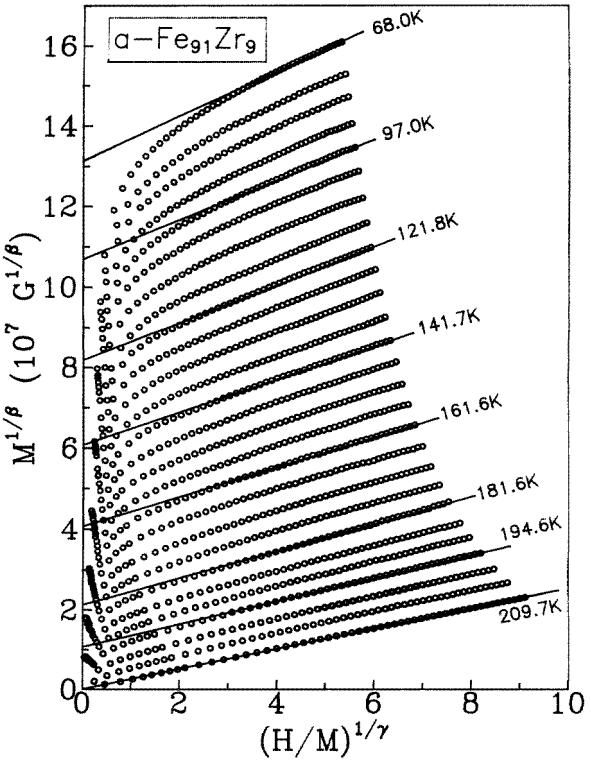

Figure 2. A modified Arrott plot for a-$Fe_{91}Zr_9$. In this plot $H \equiv H_{eff}$.

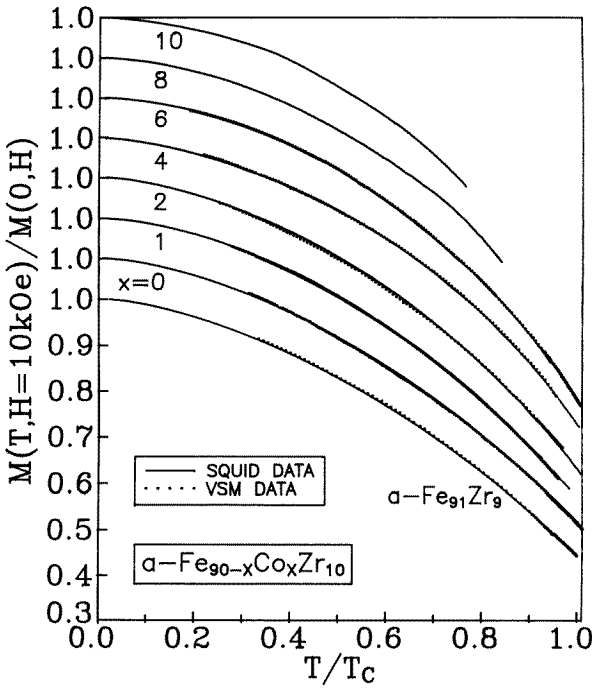

Figure 3. A comparison of the SQUID and VSM magnetization data taken at $H \equiv H_{ext} = 10$ kOe.

Table 1. The spin-wave parameters for a-$Fe_{91}Zr_9$ and a-$Fe_{90-x}Co_xZr_{10}$ alloys deduced from the SQUID magnetization data at H_{ext} = 10 kOe. The corresponding parameter values obtained from the VSM magnetization data at H_{ext} = 10 kOe are displayed within the square brackets. The numbers in parentheses denote the uncertainty in the least significant figure.

Alloy/ concentration x	t^*	$M(0, H)$ (G)	$D(0)$ (meV Å^2)	D_2 (10^{-6} K^{-2})	T_C (K)	$D(0)/T_C$ (meV Å^2 K^{-1})
$Fe_{91}Zr_9$	0.50	969(25) [930(30)]	29(2) [29(3)]	2.0(5) [1.9(5)]	209.66(5)	0.138(10)
0	0.50	1052(20) [1015(30)]	31(2) [32(3)]	1.5(5) [1.4(5)]	225.00(5)	0.137(10)
1	0.45	1120(25) [1100(30)]	35(2) [34(3)]	2.0(5) [2.0(5)]	256.66(5)	0.136(12)
2	0.45	1165(25) [1150(35)]	38(3) [36(3)]	2.5(5) [2.6(5)]	281.60(5)	0.135(14)
4	0.45	1305(20) [1280(25)]	45(3) [41(4)]	2.0(5) [2.2(5)]	327.95(5)	0.137(13)
6	0.40	1315(25) [1290(30)]	52(3) [48(5)]	3.5(8) [3.2(8)]	374.75(5)	0.142(14)
8	0.40	1343(25)	62(3)	3.5(8)	419.50(10)	0.148(8)
10	0.40	1360(25)	70(2)	3.0(8)	462.50(10)	0.152(5)

1.5 kOe $\leqslant H_{ext} \leqslant$ 15 kOe. Such sets of data are referred to as the 'in-field' magnetization or $M(T, H \equiv H_{ext})$ data in the subsequent text. Note that, for the sake of convenience, we have used H to represent both H_{ext} and H_{eff} in the text and in some figures, but a clear-cut distinction between the two has been made in the figure captions. The spontaneous magnetization at different temperatures, $M(T, 0)$, is extracted from the M versus H_{ext} isotherms as follows. The customary approach of determining $M(T, 0)$ from the intercepts on the ordinate that the linear extrapolation of the high-field portions of M^2 versus H/M isotherms to $H \equiv H_{eff} = 0$ yields has not been adopted in the present case, because slight but finite curvature in these isotherms persisting even up to the highest effective field renders such an extrapolation ambiguous. A representative M^2 versus H/M plot (with $H \equiv H_{eff}$) shown in figure 1 serves to highlight this point. This problem has been effectively tackled by constructing the modified Arrott ($M^{1/\beta}$ versus $(H/M)^{1/\gamma}$) plot (MAP) from the 'raw' M versus H_{ext} isotherms after correcting H_{ext} for demagnetization and making the choice of spontaneous magnetization and initial susceptibility critical exponents β and γ that makes the MAP isotherms a set of parallel straight lines in the asymptotic critical region. For all of the compositions studied, the critical exponents β and γ possess three-dimensional Heisenberg-like values $\beta = 0.365$ and $\gamma = 1.386$ (for details, see reference [17]). The values of the spontaneous magnetization at different temperatures are then computed from the intercepts on the ordinate (the $M^{1/\beta}$-axis) obtained by extrapolating high-field linear portions of the MAP isotherms to $H \equiv H_{eff} = 0$. This procedure is illustrated by a typical MAP displayed in figure 2.

Table 2. The parameter values and temperature ranges for the fits to the $M(H = 0, T)$ data based on equations (19), (24) and (30) of the text for the a-$Fe_{91}Zr_9$ and a-$Fe_{90-x}Co_xZr_{10}$ alloys. The values within the square brackets are the $M(0, 0)$ values obtained directly from the M versus H isotherm measured at $T = 5$ K. The numbers in parentheses denote the uncertainty in the least significant figure.

Alloy/ conc- entration x	t^*	$M(0, 0)$ (G)	$D(0)$ (meV Å^2)	D_2 (10^{-6} K^{-2})	Fitting range t^{**}–t^{***}	A (10^{-6} K^{-2})	Fitting range t'–t''	A' (10^{-4} K$^{-4/3}$)
$Fe_{91}Zr_9$	0.50	945(35) [965(30)]	28(3)	1.8(5)	0.53–0.77	15.4(2)	0.74–0.95	7.85(5)
0	0.50	1026(30) [1041(30)]	32(3)	1.7(5)	0.51–0.78	13.5(4)	0.67–0.97	7.13(8)
1	0.45	1075(35) [1100(30)]	34(3)	2.2(5)	0.44–0.71	9.7(1)	0.74–0.94	5.99(5)
2	0.45	1145(35) [1170(30)]	37(3)	2.5(5)	0.45–0.69	8.4(2)	0.67–0.95	5.30(8)
4	0.45	1275(35) [1296(30)]	44(4)	2.2(5)	0.44–0.73	6.1(1)	0.64–0.93	4.31(5)
6	0.40	1290(30) [1305(30)]	51(5)	3.0(8)	0.45–0.75	4.8(2)	0.64–0.96	3.63(4)
8		[1344(30)]				{7.6(2)}[a]		
10		[1359(30)]				{6.3(2)}[a]		

[a] Extrapolated values of the coefficient $A''(0)$ in equation (25) obtained from $A''(H)$ at $H_{ext} = 10$ kOe.

4. Data analysis, results and discussion

Figure 3 makes a detailed comparison between the reduced 'in-field' magnetization, $M(T, H)/M(0, H)$, data taken for a-$Fe_{90-x}Co_xZr_{10}$ ($x = 0$, 1, 2, 4, 6, 8 and 10) and a-$Fe_{90+y}Zr_{10-y}$ ($y = 0$, 1) alloys at different temperatures in a constant external magnetic field of $H \equiv H_{ext} = 10$ kOe using vibrating-sample and SQUID magnetometers. A remarkably good agreement between the SQUID and VSM data in the overlapping temperature range is seen in this figure. An elaborate 'range-of-fit' analysis (in which the values of free fitting parameters and the quality of the fits are continuously monitored as the temperature interval $T_{min} \leqslant T \leqslant T_{max}$ is progressively narrowed down by keeping T_{min} (T_{max}) fixed at a given value and lowering (raising) T_{max} (T_{min}) towards T_{min} (T_{max}) and whose details are given elsewhere [2, 9, 18]) of the $M(T, H)$ ($M(T, 0)$) data, based on equations (20), (24), (25) and (30) (equation (19) as well as equations (24), (25) and (30) with $H = 0$) with $D(T)$ in equation (20) (equation (19)) given by either $D(T) = D(0)(1 - D_2T^2)$ or $D(T) = D(0)(1 - D_{5/2}T^{5/2})$, has been carried out with the following results.

(i) For all of the compositions studied, the best least-squares (LS) fits to the $M(T, H)$ and $M(T, 0)$ data for temperatures $t = T/T_C \leqslant t^*$ are provided by equations (20) and (19), respectively, with $D(T)$ in these equations given by $D(T) = D(0)(1 - D_2T^2)$ and the parameter values as well as the temperature ranges for different compositions given in

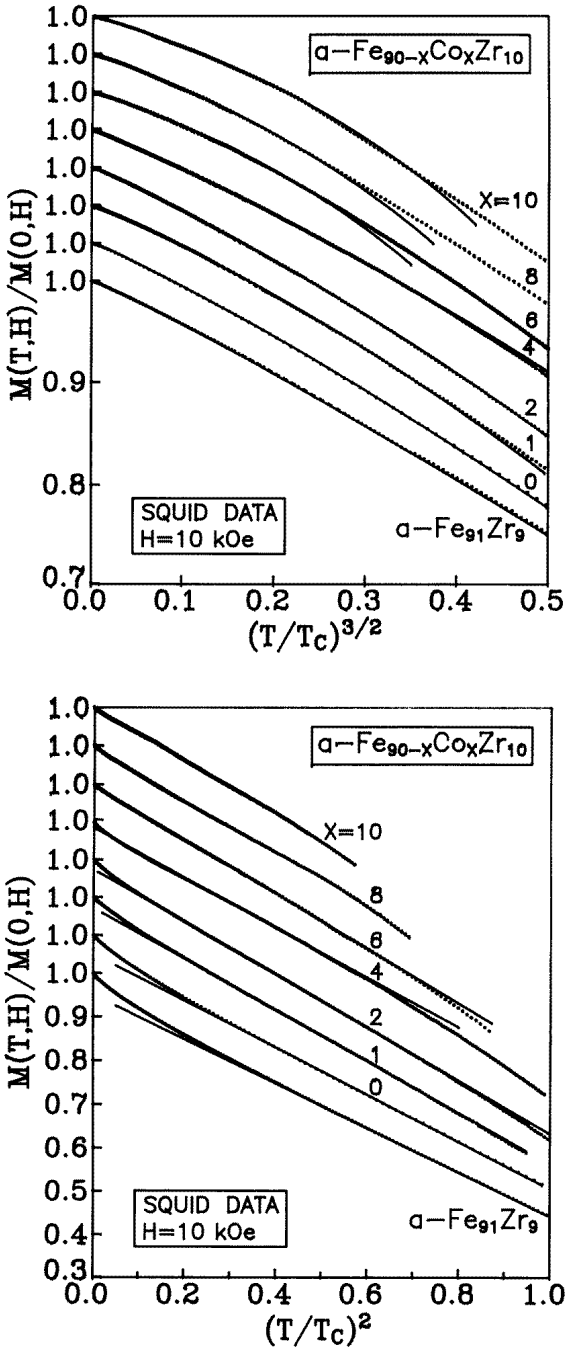

Figure 4. The reduced magnetization at $H \equiv H_{ext} = 10$ kOe versus $(T/T_C)^{3/2}$ and $(T/T_C)^2$. Continuous curves/lines denote the least-squares (LS) fits to the data based on equations (20) and (24) of the text.

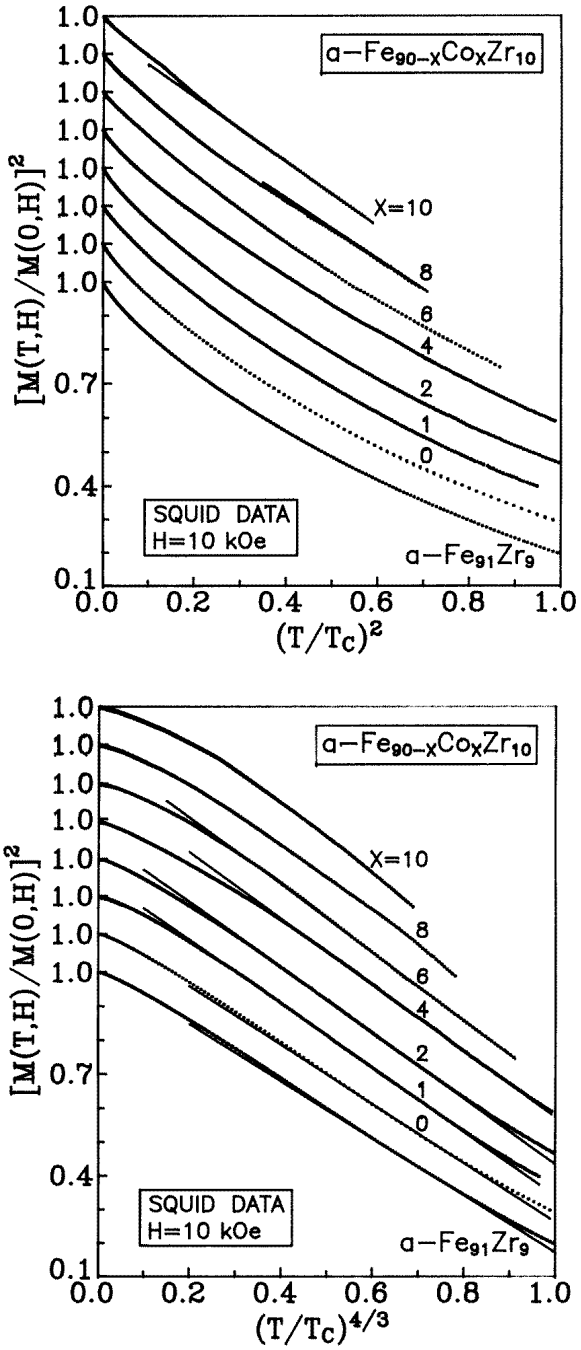

Figure 5. $[M(T,H)/M(0,H)]^2$ at $H \equiv H_{ext} = 10$ kOe as a function of $(T/T_C)^2$ and $(T/T_C)^{4/3}$. Continuous straight lines denote the LS fits to the data based on equations (30) and (25) of the text.

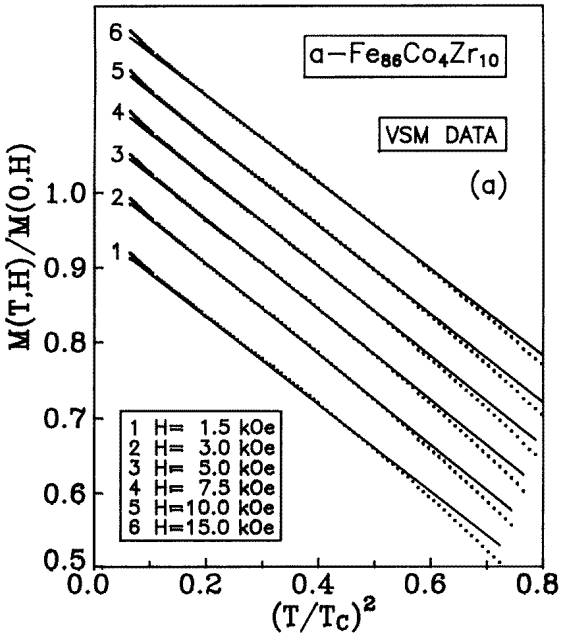

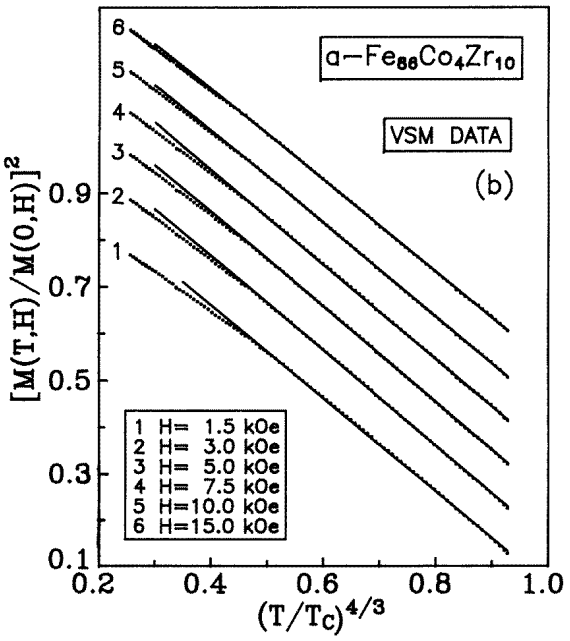

Figure 6. $M(T, H)/M(0, H)$ versus $(T/T_C)^2$ and $[M(T, H)/M(0, H)]^2$ versus $(T/T_C)^{4/3}$ plots at a few selected values of $H \equiv H_{ext}$. Continuous straight lines denote LS fits to the data based on equations (24) and (30) of the text. Note that the data denoted by the numbers 2, 3, 4, 5, 6 are shifted up by the amounts 0.05, 0.10, 0.15, 0.20, 0.25 and 0.08, 0.16, 0.24, 0.32, 0.40 with respect to data denoted by 1 in (a) and (b), respectively.

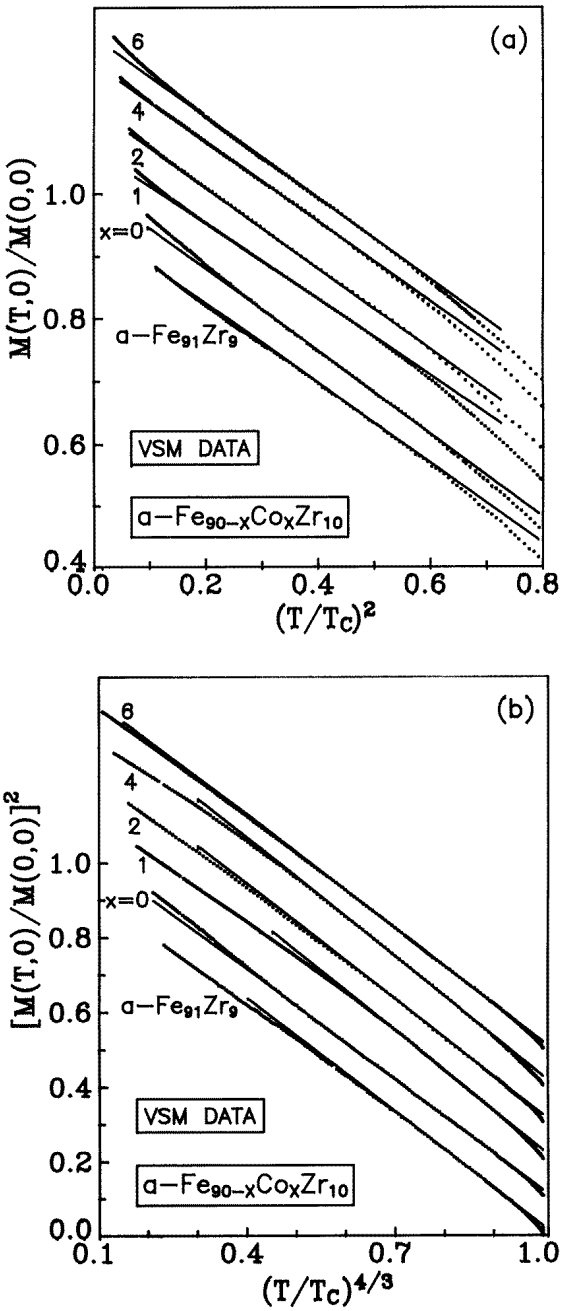

Figure 7. $M(T,0)/M(0,0)$ versus $(T/T_C)^2$ and $[M(T,0)/M(0,0)]^2$ versus $(T/T_C)^{4/3}$ plots constructed from the VSM $M(T,0)$ data. Continuous straight lines denote LS fits to the data based on equations (24) and (30) of the text with $H = 0$. Note that the data for $x = 0$, 1, 2, 4, 6 are shifted up by the amounts 0.06, 0.12, 0.18, 0.24, 0.30 and 0.10, 0.20, 0.30, 0.40, 0.50 with respect to those for a-$Fe_{91}Zr_9$ in (a) and (b), respectively.

Table 3. Parameter values and temperature ranges for the fit to the SQUID and VSM (given in square brackets) $M(T, H)$ data at H_{ext} = 10 kOe based on equations (24), (25) and (30) of the text.

Alloy/ concentration x	Fitting range t^{**}–t^{***}	A (10^{-6} K^{-2})	Fitting range $t^{\dagger}$–$t^{\dagger\dagger}$	A'' (10^{-6} K^{-2})	Fitting range t'–t''	A' (10^{-4} K$^{-4/3}$)
$Fe_{91}Zr_9$	0.58–0.98 [0.65–0.98]	12.0(2) [12.2(2)]			0.53–0.87 [0.66–0.83]	6.60(5) [6.65(5)]
0	0.55–0.91 [0.58–0.98]	11.0(3) [11.2(2)]			0.62–0.84 [0.62–0.84]	6.12(8) [6.22(8)]
1	0.53–0.92 [0.55–0.95]	9.2(1) [9.2(2)]			0.50–0.82 [0.50–0.85]	5.50(5) [5.46(4)]
2	0.49–0.84 [0.45–0.89]	7.8(3) [7.6(2)]			0.46–0.79 [0.50–0.80]	4.94(8) [4.85(5)]
4	0.40–0.69 [0.40–0.75]	5.4(2) [5.5(1)]			0.56–0.93 [0.56–0.93]	3.90(5) [3.98(4)]
6	0.44–0.79 [0.45–0.78]	4.5(2) [4.4(1)]			0.70–0.90 [0.55–0.87]	3.44(4) [3.41(3)]
8			0.74–0.83	5.45(5)		
10			0.53–0.75	4.72(5)		

tables 1 and 2; table 1 also includes the corresponding values for the VSM data taken at $H_{ext} = 10$ kOe within the square brackets.

(ii) $M(T, H)$ and $M(T, 0)$ for the alloys with $x \leqslant 6$ and $y = 0$, 1 are best described by equation (24) with $H \neq 0$ and $H = 0$, respectively, over the intermediate-temperature range $t^{**} \leqslant t \leqslant t^{***}$, while equation (30) with $H \neq 0$ and $H = 0$ yields the best LS fits to the $M(T, H)$ and $M(T, 0)$ data for temperatures close to T_C in the interval $t' \leqslant t \leqslant t''$; the values for different parameters and the temperature ranges for such fits are listed in tables 2 and 3. In sharp contrast with this behaviour, equation (25) reproduces the observed temperature variation of the magnetization for the alloys with $x = 8$ and 10 more accurately in the range $t^{\dagger} \leqslant t \leqslant t^{\dagger\dagger}$ than equation (24). The different types of fit to the $M(T, H)$ and $M(T, 0)$ data mentioned above are represented in figures 4–7 by continuous curves or straight lines.

(iii) The VSM and SQUID data taken at $H_{ext} = 10$ kOe yield identical results (tables 1 and 3). In this context, it is gratifying to note that even though the VSM data for temperatures below 68 K, which are crucial to an accurate determination of the spin-wave (SW) parameters such as $D(0)$ and D_2, are not currently available, the fits to the VSM and SQUID data, based on equation (20), give the same values (within the uncertainty limits) for these parameters as well as for $M(0, H)$. Moreover, the values for the SW parameters (tables 1 and 2) deduced from the VSM $M(T, H)$ and $M(T, 0)$ data, available only for $T \geqslant 68$ K, conform well with one another.

(iv) The coefficients A and A' of the T^2- and $T^{4/3}$-terms in equations (24) and (30) decrease with increasing H_{ext} for a given composition and with increasing Co concentration for a given field value (figure 8).

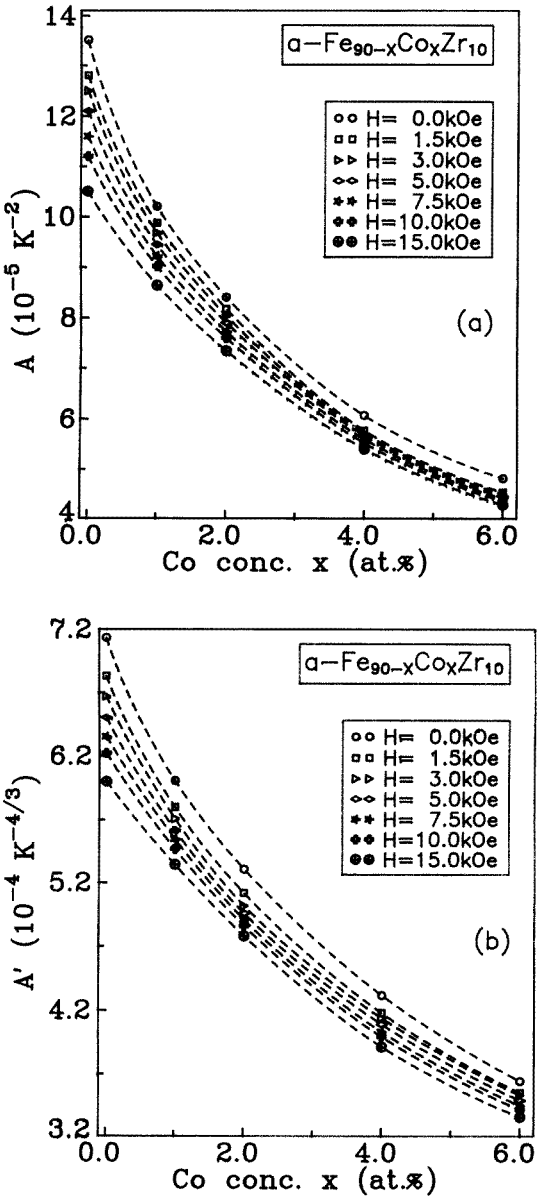

Figure 8. The concentration dependence of the coefficients A and A' appearing in equations (24) and (30) of the text at a few selected values of $H \equiv H_{ext}$.

Before discussing the above results under appropriate subheadings, other findings, which have a direct bearing on these results, are mentioned in the text that follows.

4.1. Irreversibility in magnetization at low fields and temperatures

Figure 9 displays the thermomagnetic scans for a-$Fe_{91}Zr_9$, a-$Fe_{90}Zr_{10}$ and a-$Fe_{89}Co_1Zr_{10}$ alloys taken at $H_{ext} = 10$ Oe. In this figure, open circles and closed squares represent

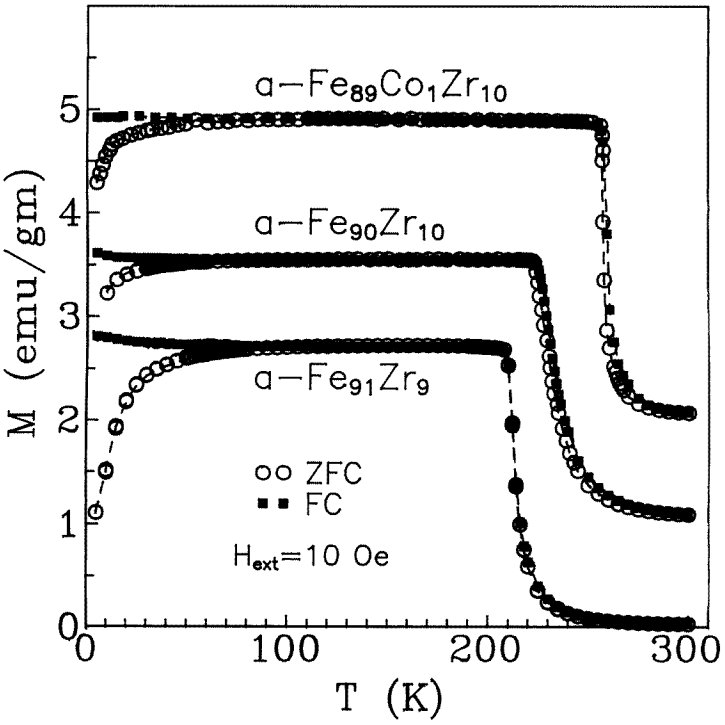

Figure 9. Thermomagnetic scans for a-$Fe_{91}Zr_9$, a-$Fe_{90}Zr_{10}$ and a-$Fe_{89}Co_1Zr_{10}$ alloys at $H \equiv H_{ext} = 10$ Oe.

the data obtained when the magnetization at $H_{ext} = 10$ Oe is measured as a function of temperature while heating the sample from 4.2 K after it had been cooled to 4.2 K in *zero field* from 300 K (i.e., the zero-field-cooled magnetization, $M_{ZFC}(T)$) and while cooling the sample from 300 K (i.e., the field-cooled magnetization, $M_{FC}(T)$), respectively. The important features that these scans present are as follows.

(a) A steep rise followed by saturation in magnetization as the temperature is lowered below a certain temperature, and the appearance of a 'kink' in $M(T)$ at a temperature $T_{kink} \simeq T_C$ signalling the onset of long-range ferromagnetic order.

(b) A bifurcation of the $M_{ZFC}(T)$ and $M_{FC}(T)$ curves at a temperature T_{RE} (called the re-entrant temperature).

(c) A 'knee' in the $M_{ZFC}(T)$ curve at a temperature T_f (the so-called freezing temperature).

The main findings based on similar scans taken at different fixed field values for various compositions in the alloy series a-$Fe_{90-x}Co_xZr_{10}$ and a-$Fe_{90+y}Zr_{10-y}$ are summarized as follows.

(i) For a given composition, T_{kink}, T_{RE} and T_f decrease with increasing H_{ext}—so much so that for $H_{ext} \geqslant 500$ Oe the bifurcation in the magnetization curves completely disappears (alternatively, T_{RE} and T_f are reduced to values <4.2 K).

(ii) For a specified but fixed value of H_{ext}, T_{kink} increases while T_{RE} and T_f decrease with increasing x (or decreasing y) such that the irreversibility of the magnetization is

completely suppressed for $x \geqslant 6$. For instance, at $H_{ext} = 10$ Oe, $T_{kink} = 209(1)$ K, 225(1) K, 255(1) K, 282(1) K, $T_{RE} = 85(5)$ K, 60(5) K, 45(5) K, 30(5) K and $T_f = 30(3)$ K, 20(2) K, 8(1) K, 5.5(5) K for a-$Fe_{91}Zr_9$, a-$Fe_{90}Zr_{10}$, a-$Fe_{89}Co_1Zr_{10}$, a-$Fe_{88}Co_2Zr_{10}$ alloys, respectively; $T_{kink} > 328(1)$ K, $T_{RE} = 15(5)$ K and $T_f < 4.2$ K for a-$Fe_{86}Co_4Zr_{10}$.

Apart from these findings, asymmetric hysteresis loops, isoremanent and thermoremanent effects, and an exponential increase in coercivity, i.e., properties characteristic of the cluster spin-glass (or mictomagnetic) state, have been observed for the alloys with $y = 0$, 1 in the a-$Fe_{90+y}Zr_{10-y}$ series and $x \leqslant 2$ in the a-$Fe_{90-x}Co_xZr_{10}$ series at $T < T_{RE}$. However, these properties occur in association with *finite* spontaneous magnetization, indicating thereby that the magnetic state for $T < T_{RE}$ is a *mixed* state in which long-range ferromagnetic order coexists with cluster spin-glass order. Observations similar to those mentioned above have also been made previously [1, 3, 19–21] for glassy alloys with the same or similar nominal composition.

The above observations find a straightforward but qualitative explanation in terms of the *infinite* three-dimensional (3D) ferromagnetic (FM) matrix plus *finite* FM spin-clusters model (henceforth referred to as the K model) proposed by Kaul for amorphous ferromagnets and whose details are given elsewhere [2, 3, 22]. In this phenomenological model, it is postulated that:

(A) the spin system for $T < T_C$ consists of an infinite 3D FM matrix and finite spin clusters (composed of a set of ferromagnetically coupled spins), which are embedded in, but 'isolated' from, the FM matrix by zones of frustrated spins surrounding the finite clusters,

(B) a wide distribution in the size of clusters exists, and

(C) the spin clusters are not completely isolated in that long-range Ruderman–Kittel–Kasuya–Yosida (RKKY) interactions provide a *weak* coupling not only between the finite clusters and the FM matrix but also between the clusters themselves.

Since the average inter-atomic spacing in the finite FM clusters with *bcc-like* atomic short-range order (SRO) ('*low-density* pockets') is *much larger* [2] than that in the infinite FM matrix with *fcc-like* atomic SRO ('*high-density* bulk'), magnetic moments (spins) in the clusters have *localized* character whereas those in the FM matrix are *itinerant*. The existence of both localized as well as the itinerant type of magnetic electron in these systems was proposed by one of the authors [1] long ago. In this picture, a 'mixed magnetic state' comes into existence when the weakly interacting finite spin clusters *freeze* (the freezing process in not cooperative in the sense that not all of the clusters freeze at the same temperature; freezing occurs over an extended range of temperatures [3] because of the distribution in cluster size and hence in cluster relaxation times) in random orientations and *coexist* with the (*itinerant*) FM matrix for temperatures below T_{RE}. In the mixed state, the coercivity increases steeply [23], particularly for $T < T_f$, as a result of the pinning of domain walls by the frozen FM clusters embedded in the FM matrix. The irreversibility of the low-field magnetization at low temperatures and the precipitous decline in M_{ZFC} for $T < T_f$ can be satisfactorily explained by properly correcting [24] for the self-demagnetizing effects brought about by the presence of the exponentially increasing coercivity and the concomitant magnetic hardness (magnetic anisotropy energy). By contrast, the transverse spin-freezing (TSF) model [25], which is similar to the Gabay–Toulouse (GT) mean-field model [26] for Heisenberg spins, fails to account for the steep fall in M_{ZFC} for $T < T_f$ unless this model is modified to include anisotropy effects [27–29] which come into play for temperatures below T_f.

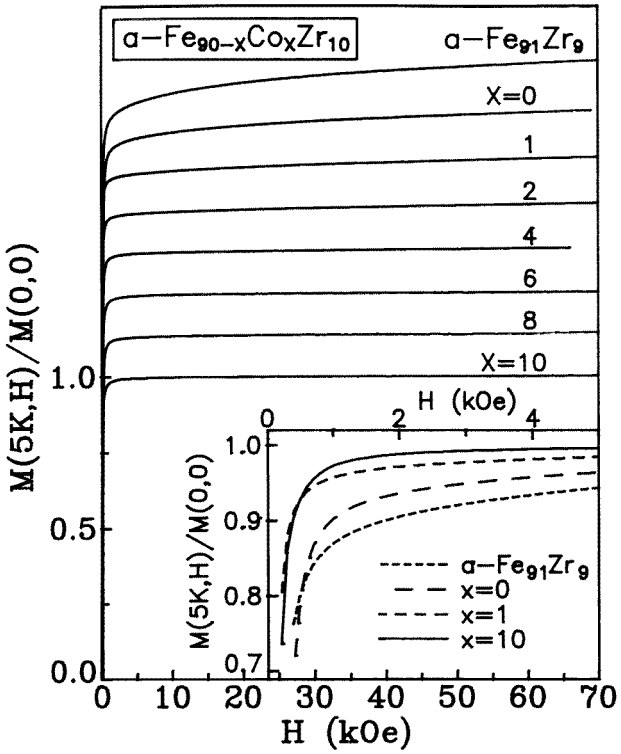

Figure 10. M versus $H \equiv H_{ext}$ curves taken at $T = 5$ K; for the sake of clarity, the curves for $x = 8$, 6, 4, 2, 1, 0 and a-$Fe_{91}Zr_9$ are shifted up by the amounts 0.1375, 0.275, 0.4125, 0.552, 0.6875, 0.825 and 0.9625 with respect to the one for x = 10, respectively. The inset shows the variation of the reduced magnetization with H_{ext} for $H_{ext} \leqslant 4.5$ kOe.

4.2. High-field susceptibility at 0 K

The magnetization, $M(T, H)$, data taken at $T = 5$ K in applied fields up to 70 kOe for a-$Fe_{91}Zr_9$ and a-$Fe_{90-x}Co_xZr_{10}$ ($0 \leqslant x \leqslant 10$) alloys using the SQUID magnetometer are plotted in the form of $M(0, H)/M(0, 0)$ versus H ($\equiv H_{ext}$) curves in figure 10. Note that no distinction has been made between the values of the magnetization at 5 K and 0 K in this figure and in figures 3–9. The differential susceptibility, $\chi(0, H) \equiv \mathrm{d}M(0, H)/\mathrm{d}H$, as a function of H ($\equiv H_{ext}$) for fields well above the technical saturation, obtained by numerical differentiation of these M versus H_{ext} curves, is shown in figure 11. A close examination of the data presented in these figures reveals that for all of the alloys investigated (particularly those with low Co content), the magnetization does not saturate even in fields as high as 70 kOe and that $\chi(0, H)$ gradually decreases with increasing H_{ext} and approaches a constant value at high fields. This limiting value is simply the high-field susceptibility, χ_{hf}. The inset of figure 11 shows χ_{hf} plotted against the Co concentration, x. As the Co concentration is increased, the plateau in the $\chi(0, H)$ versus H_{ext} curve is reached at a lower field value and concomitantly the field at which technical saturation of the magnetization occurs also shifts to lower values (see the inset of figure 10) while χ_{hf} decreases rapidly for $x < 4$, and this decreasing trend slows down considerably for $x > 6$ (see the inset of figure 11). The value of the spontaneous magnetization at 0 K, $M(0, 0)$, is then obtained by subtracting $\chi_{hf} H_{ext}$ from

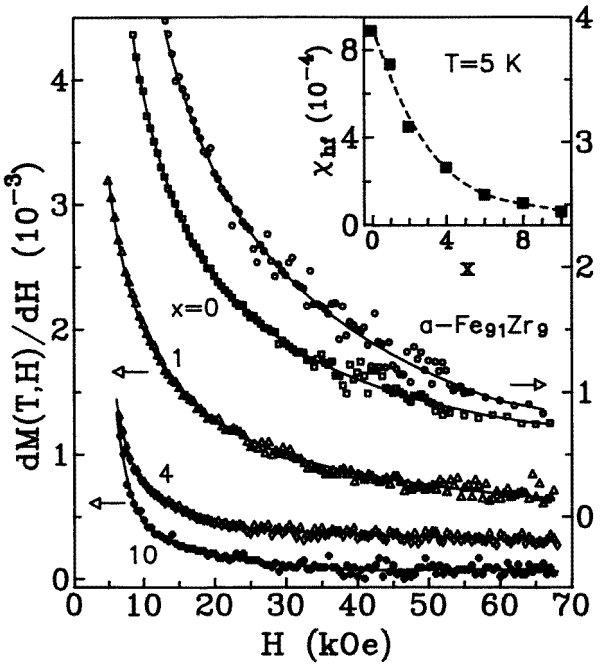

Figure 11. The differential susceptibility as a function of $H \equiv H_{ext}$. The inset shows the variation of χ_{hf} with x. Note that the error bars for χ_{hf} are smaller than the size of the symbols and the smooth curves (the dashed curve in the inset) serve as a guide to the eye.

Table 4. Band and exchange parameters.

Alloy/ concentration x	μ_0 (μ_B)	χ_{hf} (10^{-4})	$\chi(0,0)$ (10^{-4})	S	$IN(E_F)$	$N(E_F)$[a] (eV^{-1})	I (eV)
$Fe_{91}Zr_9$	1.34(2)	12.32(10)	14.00(20)	83(1)	1.012(1)	4.00	0.25(1)
0	1.44(2)	8.86(20)	10.37(20)	66(1)	1.015(1)	3.74	0.27(1)
1	1.52(2)	7.32(15)	7.78(10)	53(1)	1.019(1)	3.49	0.29(1)
2	1.62(2)	4.47(15)	4.72(10)	34(2)	1.029(1)	3.30	0.31(1)
4	1.79(2)	2.61(10)	2.97(10)	24(1)	1.042(1)	3.00	0.35(1)
6	1.81(2)	1.38(10)	1.50(10)	13(1)	1.079(4)	2.82	0.38(1)
8	1.82(2)	1.00(15)	1.34(10)	12(1)	1.084(5)	2.70	0.40(1)
10	1.84(2)	0.60(20)	0.64(10)	6(1)	1.170(23)	2.61	0.45(1)

[a] References [45] and [46].

$M(T, H_{ext})$ at $H_{ext} = 70$ kOe. The values of $M(0,0)$ and χ_{hf} for different compositions so obtained are listed in tables 2 and 4, respectively. As we shall show in the following subsection, all of the above observations, including the Co concentration dependence of χ_{hf} and $M(0,0)$, find a simple qualitative interpretation in terms of the K and SF models.

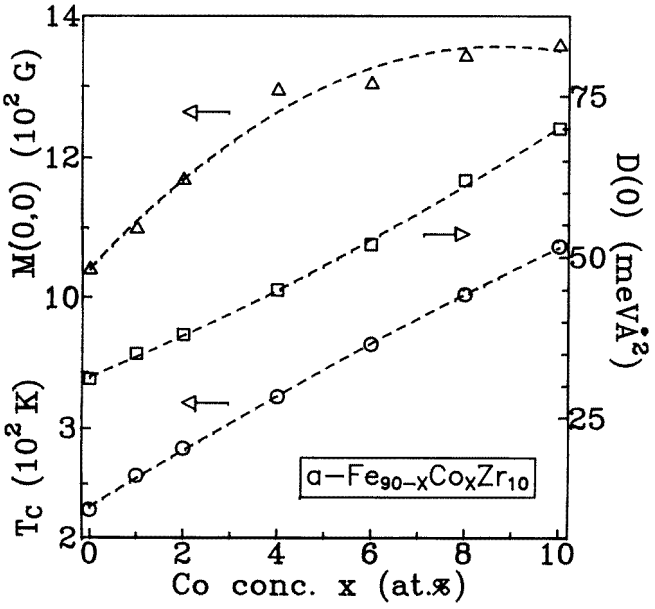

Figure 12. The variation of T_C, $D(0)$ and $M(0, 0)$ with the Co concentration.

4.3. Spin-wave excitations

The main observations of the present study in the low-temperature region are as follows.

(i) In a-$Fe_{90-x}Co_xZr_{10}$ and a-$Fe_{90+y}Zr_{10-y}$ alloys, spin-wave excitations give the dominant contribution to the thermal demagnetization of both the spontaneous and the 'in-field' magnetization for temperatures below t^*, which ranges between 0.5 and 0.4 for the alloys with $0 \leqslant x \leqslant 10$ and $0 \leqslant y \leqslant 1$. The values of $M(0, H)$ and $M(0, 0)$ obtained from the best LS fits are in good agreement (within the uncertainty limits) with those actually measured at $T = 5$ K. Such a close agreement particularly in the case of $M(T, 0)$ is gratifying considering that $M(T, 0)$ for all of the alloys in the present study was determined for $T \geqslant 68$ K only.

(ii) The temperature dependence of the spin-wave stiffness 'D' cannot be ignored and $D(T)$ renormalizes with temperature in accordance with the expression $D(T) = D(0)(1 - D_2T^2)$, predicted by the itinerant-electron model for all of the compositions studied.

(iii) Contrary to an earlier claim [23, 30], the spin-wave stiffness at 0 K, $D(0)$, does *not depend* on the external magnetic field.

(iv) The $D(0)/T_C$ ratio for the alloys with $x \leqslant 6$ and $y \leqslant 1$ possesses a value close to 0.14, which is typical for amorphous alloys with competing interactions, while for the alloys with x = 8 and 10, $D(0)/T_C > 0.14$. T_C and $D(0)$ increase more or less linearly with x while the steep rise in $M(0, 0)$ observed for $x \lesssim 4$ slows down considerably beyond $x = 6$—so much so that $M(0, 0)$ remains nearly constant for higher Co concentrations (see figure 12).

The existence of well-defined spin-wave excitations at low temperatures (observation (i)) can be understood in terms of both localized as well as itinerant-electron models. However, observation (ii) provides evidence for itinerant behaviour of magnetic electrons in

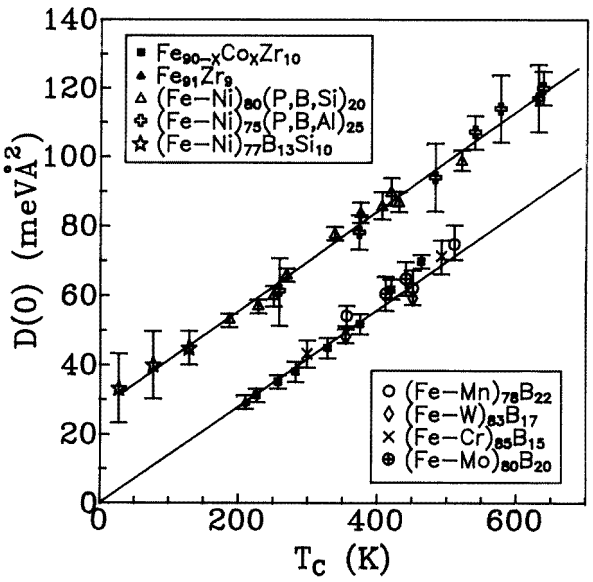

Figure 13. $D(0)$ versus T_C for a-$Fe_{91}Zr_9$ and a-$Fe_{90-x}Co_xZr_{10}$ alloys. Similar data for other systems available in the literature [32–37] are also included for comparison.

the alloys in question and indicates that the magnon–spin-fluctuation interactions dominate over magnon–magnon interactions. The values of $D(0)$ deduced from the $M(T, 0)$ and $M(T, H)$ data conform very well with one another. However, at low temperatures, the $M(T, 0)$ data yield a *lower* value of $D(0)$ than that obtained from the $M(T, H)$ data for the alloys with $x \lesssim 4$, $y \leqslant 1$ as already reported [2] for a-$Fe_{90\pm y}Zr_{10\mp y}$ alloys. This discrepancy in the values of $D(0)$ should *not* be taken to imply that $D(0)$ is field dependent, but the reduced value of $D(0)$ should be viewed as signalling the softening of spin-wave modes [2, 3, 31] in the re-entrant state (in which long-range ferromagnetic order coexists with cluster spin-glass order) which comes into existence at temperatures $T \leqslant T_{RE}$, well below T_C, in these alloys [1, 3, 19]. In the present work, we do not observe the softening of spin-wave modes for the alloys with $x < 4$ and $y \leqslant 1$ because the $M(T, 0)$ data in the present case are available only for $T \geqslant 68$ K, a temperature well above the re-entrant temperature, T_{RE}. For $x > 6$, such a behaviour is not expected since the re-entrant behaviour is completely suppressed when $x \simeq 6$ (subsection 4.1). In view of the *field-independent* value of $D(0)$, the dependence of $D(0)$ on H reported [23, 30] earlier could be an artifact of the analysis which attributes the observed thermal demagnetization to either a spin-wave or a single-particle contribution alone and neither takes into account the temperature renormalization of D nor corrects for the gap in the spin-wave spectrum arising from the applied field. The plot of $D(0)$ versus T_C for the alloys investigated here, shown in figure 13, also includes the $D(0)$ data for several 3d-transition-metal–metalloid amorphous alloys available in the literature [32–37]. According to a theoretical prediction [32] based on the Heisenberg model, the values of $D(0)$ for amorphous ferromagnetic alloys, when plotted against T_C, should fall on a straight line represented by

$$D(0) = D_0 + mT_C \tag{31}$$

where $m = 0.144$ meV Å^2 K^{-1} and D_0 is either finite or zero depending on whether the exchange interactions extend beyond the nearest-neighbour (NN) distance or not. It can

be noticed from figure 13 that the values of $D(0)$ for a-(Fe, M)–B alloys (M = Cr, Mn, W) [33–35], in which competing interactions are known to be present, fall on a straight line with slope $m = 0.144$ meV Å^2 K^{-1} that passes through the origin, whereas the values of $D(0)$ for a-(Fe, Ni)–M (M = P, B, Si, Al) alloys [32, 36, 37] fall on a different straight line, parallel to the other one, but with the finite intercept $D_0 = 24 \pm 3$ meV Å^2. This implies that the competing interactions present in the former set of amorphous alloys restrict the range of exchange interactions to the nearest neighbours only, whereas the direct exchange interactions extend to the next-nearest neighbours in the latter set. Following these arguments, the values of $D(0)$ for the alloys with $0 \leqslant x \leqslant 6$, $y \leqslant 1$ fall on the straight line with $m = 0.144$ meV Å^2 K^{-1} and $D_0 = 0$, indicating thereby that the *competing* interactions present in these alloys confine the direct exchange interactions to nearest neighbours only. With increasing Co concentration, the competing interactions are gradually suppressed and, for the alloys with $x > 6$, the $D(0)$ values depart from this straight line and approach the line with the finite intercept. This observation implies that exchange interactions in these alloys extend beyond the NN distance.

A linear relation between $D(0)$ and T_C of the type $D(0) = mT_C$ is also predicted by the theory based on the itinerant-electron model due to Katsuki and Wohlfarth [38]. With the assumption that the Curie temperature T_C is determined by the Stoner single-particle excitations alone, Katsuki and Wohlfarth [38] derived for weak itinerant ferromagnets the following relation between $D(0)$ and T_C:

$$D(0) = k_B T_C a^2 f(n) \tag{32}$$

where a is the nearest-neighbour (NN) distance and $f(n)$ is a function of the number of electrons per atom determined by the band structure. When the effective-mass approximation is used, equation (32) reduces to [38]

$$D(0) = (\pi k_B / 6\sqrt{2} k_F^2) T_C \tag{33}$$

where k_F is the Fermi wave vector. The typical value $k_F = 1.5$ Å^{-1}, when inserted into equation (33), yields the value of the slope (m) as 0.014 meV Å^2 K^{-1}. This slope value is exactly one order of magnitude smaller than the observed one. Such a large discrepancy between theory and experiment is not surprising in view of the fact that the assumptions—namely, (i) that T_C is determined by single-particle excitations alone and (ii) the effective-mass approximation—on which the above theory rests are not valid in the present case. It is well known that even for weak itinerant ferromagnets the Stoner theory, which regards the single-particle excitations as the sole cause of thermal demagnetization in such systems, invariably *overestimates* T_C and that this theory has to be modified to include the effect of local spin-density fluctuations on the thermal demagnetization if a correct estimate of T_C and a proper description of the Curie–Weiss behaviour of the magnetic susceptibility for $T > T_C$ is sought. The spin-fluctuation model too predicts a linear relation between $D(0)$ and T_C, of the form

$$D(0) = \{0.419 g \mu_B k_B [M(0,0)]^{-1/2} (\hbar \gamma')^{-1/4}\} T_C. \tag{34}$$

Unfortunately, due to the non-availability of the actual value of the band parameter γ', $D(0)/T_C$ cannot be estimated. However, the values of $\hbar\gamma'$ for the systems in question computed from equation (34) using the values of $M(0, 0)$ and the $D(0)/T_C$ ratio determined in this work (as well as the FMR value [16] of g) turn out to be reasonable ($\sim\mu$eV Å^{-1}).

The strong evidence for the existence of well-defined spin-wave excitations in the amorphous alloys in question provided by the present magnetization measurements is in direct contradiction with the earlier claim [4], based on INS experiments, that no propagating

features, indicative of spin waves, are observed in the constant-q scans at any temperature below T_C in the wave-vector-transfer range 0.05 Å$^{-1} \leqslant q \leqslant$ 0.12 Å^{-1} for a-$Fe_{90\pm y}Zr_{10\mp y}$ alloys. As shown below, both the K and SF (spin-fluctuation) models help in resolving this apparent contradiction.

Within the framework of the K model, the following explanation [2] can be offered for the absence [4] of spin-wave-like features in the INS spectra taken for a certain wave-vector-transfer range. Though spin waves of different wave vectors are excited in the infinite FM matrix at temperatures $T < T_C$, not all of them propagate through the matrix unhindered for the following reasons. The spin waves for which q falls within the range $q_{c1} \leqslant q \leqslant q_{c2}$, where q_{c1} and q_{c2} are the caliper dimensions of the smallest (largest) and the largest (smallest) spin cluster in the wave-vector (direct) space, get *severely damped* due to coupling to, and intense scattering from, the finite spin clusters. These *overdamped* modes manifest themselves as *non-propagating* spin fluctuations of the type mentioned in section 2. Therefore, if the INS measurements are performed for the wave-vector range $q_{c1} \leqslant q \leqslant q_{c2}$, only a broad 'diffusive-like' spectrum with no propagating features would be observed at any temperature below T_C. By contrast, constant-q scans recorded at the wave-vector values that lie outside this q-range should exhibit well-defined spin-wave peaks for all temperatures below T_C, but the nature and origin of these spin waves now depend on whether $q < q_{c1}$ or $q > q_{c2}$. In the long-wavelength limit (i.e., when $q < q_{c1}$), well-defined spin waves can be excited in the FM matrix only, and that too at temperatures well below T_C because of the low energy cost involved, and such spin waves propagate through the matrix without any significant damping. On the other hand, in the short-wavelength limit (i.e., when $q > q_{c2}$), spin waves can be excited in the FM matrix as well as in the finite clusters—in the latter case, either at very high incident neutron energies when the temperature is low or at high temperatures for the range of incident neutron energies conventionally used. However, in this case (i.e., when $q > q_{c2}$), the spin waves in the FM matrix are expected to get damped due to strong fluctuations in the *local* magnetization and the *local* density of states (DOS) (caused by topological disorder) as contrasted with the intra-cluster spin waves which should be relatively well defined because both the local magnetization and the local DOS possess larger values and have a much narrower distribution. Thus, the INS spectra should consist of reasonably sharp spin-wave peaks signalling the existence of intra-cluster spin-wave excitations superposed on very broad 'diffusive-like' structure arising from the overdamped spin waves (or more precisely, from the non-propagating spin fluctuations) in the FM matrix. In view of the earlier finding [4, 39] that in a-$Fe_{90\pm y}Zr_{10\mp y}$ alloys the *average* cluster size for $T \lesssim T_C$ ranges between 25 Å and 200 Å, the range of q-values (0.05 Å$^{-1} \leqslant q \leqslant$ 0.12 Å^{-1}) covered in the INS experiments [4] falls well within the range $q_{c1} \leqslant q \leqslant q_{c2}$ and hence no resolvable spin-wave peaks are found in the INS spectra. In view of the foregoing arguments, the INS measurements for $T < T_C$ need to be extended to q-values *low enough* ($q \ll 0.05$ Å^{-1}; $q \to 0$) for one to observe well-defined spin waves, characteristic of the 3D FM matrix.

Unlike the Heisenberg model (which predicts that spin waves (SW) occupy the entire Brillouin zone and hence that SW are the only low-lying magnetic excitations possible), the SF model [11, 40] asserts that spin waves occupy only a small portion of the Brillouin zone (BZ) near $q = 0$ (say $q \leqslant q_{SW}$) while Stoner single-particle excitations and spin fluctuations occupy the rest. Therefore, no features in the constant-q INS scans attributable to spin waves are expected to occur when the q-range over which such measurements are carried out lies well above q_{SW}. While the predictions of both the K and SF models are consistent with the observed behaviour and both of the models assert that well-defined spin waves in these materials should be observed at all temperatures below T_C in the limit $q \to 0$,

the *homogeneous* TSF model [25] does not offer any explanation for the absence of SW peaks in the INS spectra taken over a certain q-range, mainly because it is based on the Heisenberg model which predicts that spin waves should be observable for q-values in the range $0 \leqslant q \leqslant q_{BZ}$ (the average radius of the Brillouin zone).

A progressive replacement of Fe by Co in a-$Fe_{90-x}Co_xZr_{10}$ alloys gradually evens out the local (atomic) density fluctuations [2, 3] by favouring fcc-like atomic SRO throughout the sample. This, in turn, leads to the breaking up of finite spin clusters into smaller ones and the merging of some of them with the infinite FM matrix. Hence, as the Co concentration is increased, the number of spins within the FM matrix increases at the expense of those forming finite clusters, finite clusters shrink in size and decrease in number, the cluster size distribution narrows down and the spins within the FM matrix tend towards a collinear configuration. As a consequence, the magnetization and the exchange splitting of the d sub-bands increase (hence both $D(0)$ and T_C also assume higher values, in conformity with observation (v) mentioned above) and the spin system becomes more and more homogeneous with increasing Co concentration. This implies that the range $q_{c1} \leqslant q \leqslant q_{c2}$ gradually narrows down and shifts to higher q-values with increasing Co concentration, and so finally disappears at some value of x. These arguments assert that, if the INS experiments for the same range of q-values as used earlier [4] are performed on a-$Fe_{90-x}Co_xZr_{10}$ alloys, the constant-q scans exhibiting broad diffusive-like structure at zero or even low Co concentrations should gradually acquire the propagating features indicative of well-defined long-wavelength spin-wave excitations even in this wave-vector-transfer range at higher Co concentrations.

Such a behaviour has indeed been observed recently [5] for the INS spectra taken over the above-mentioned q-range for the homologous alloy series a-$Fe_{90-x}Ni_xZr_{10}$. Due to the local random anisotropy fields that come into play when spin clusters have frozen-in random orientations [2] at $T < T_f$, the itinerant spins of the FM matrix get canted, particularly in the alloys with $x \approx y \approx 0$. The canted spin arrangement, in turn, reduces the net exchange coupling between the the FM matrix spins, leading to softening of FM spin-wave modes, and makes the saturation in the magnetization extremely difficult to achieve even at fields as high as [23, 30] 150 kOe and temperatures as low as 4.2 K. As already stated above, the effect of increasing the Co concentration is to progressively (a) shift T_f to lower temperatures (primarily due to a progressive reduction in the average cluster size and a narrower cluster size distribution), (b) make the spin arrangement collinear and (c) suppress the re-entrant behaviour at low temperatures. This explains the sharp rise in spontaneous magnetization at 0 K, $M_S \equiv M(0,0)$, for compositions $x \lesssim 4$ and the slower increase or even saturation exhibited by the $M_S(x)$ curve at higher Co concentrations (figure 12). The above arguments also provide a straightforward interpretation for the observation (from figure 10 and the inset of figure 11) that, at low temperatures, the technical saturation in the magnetization is achieved at lower fields for compositions $x > 4$ than for $x \lesssim 4$ and that χ_{hf} decreases rapidly with increasing x for $x < 6$ but remains essentially constant for $x > 6$. However, as we will show in the following subsection, spin canting is *not* the *only* cause for large values of χ_{hf} for the alloys with $x \approx y \approx 0$; a progressive suppression of weak itinerant ferromagnetism with Co substitution accounts, for the most part, for the observed functional dependence of χ_{hf} on x.

Another consequence of the non-collinear ground-state spin arrangement in a-$Fe_{90-x}Co_xZr_{10}$ and a-$Fe_{90+y}Zr_{10-y}$ alloys with $x \lesssim 6$ and $y \lesssim 1$ is that the diffusive modes associated with the longitudinal component of the magnetization ('diffusons') do contribute, besides magnons, to the $T^{3/2}$-decrease of the magnetization, equation (21), and thereby *lower* the spin-wave stiffness coefficient, $D_M(0)$, in magnitude compared to the

value that $D_M(0)$ possesses when such a contribution (due to diffusons) is totally absent, as happens to be the case for collinear ferromagnets. Considering that diffusons give rise to an elastic peak [14] in the INS spectra, the value of the spin-wave stiffness determined from such measurements, i.e., $D_N(0)$, should greatly exceed $D_M(0)$ for these systems. Such a disparity between $D_N(0)$ and $D_M(0)$ is expected to reduce continuously with decreasing y or increasing x as the spin orientations tend towards a collinear configuration. This process continues until a value of x is reached beyond which $D_N(0)$ equals $D_M(0)$, because by then the non-collinearity is fully suppressed. This prediction needs to be verified by INS measurements performed at very low q ($q \ll 0.05$ Å^{-1}) for a-$Fe_{90-x}Co_xZr_{10}$ alloys.

It should be emphasized at this stage that a progressive suppression of the Invar effect and re-entrant behaviour with Co substitution is *accompanied* by an increase of $D_M(0)$ towards $D_N(0)$ and an enhancement of both $D_M(0)$ and $D_N(0)$ such that the difference $D_N(0) - D_M(0)$ diminishes in magnitude as x increases.

Yet another interesting aspect of spin waves in weak itinerant ferromagnets is that in the absence of any spin-dependent (spin–orbit or magnetic) impurity scattering process, *spin diffusion* provides the sole intrinsic mechanism for relaxation of the long-wavelength, low-frequency modes of spin-density fluctuations. This diffusive relaxation causes a damping of spin waves (proportional to the spin-diffusion constant) which is temperature independent and varies with q as [41] q^4. Consistent with this theoretical result, recent INS experiments on the spin dynamics of amorphous $Fe_{90-x}Ni_xZr_{10}$ alloys have revealed a temperature-independent spin-wave linewidth which exhibits a q^4- or q^5-dependence. Temperature-independent spin-wave damping proportional to q^5 is also predicted by the random Heisenberg model of localized spins [42, 43] in which damping of spin waves arises from the scattering of magnons from fluctuations in the exchange interaction, but this damping mechanism yields a value for the magnon linewidth which is an order of magnitude *smaller* than the observed values.

4.4. Spin fluctuations

The main observations for the intermediate-temperature range ($t^{**} \leqslant t \leqslant t^{***}$) and for temperatures close to T_C ($t' \leqslant t \leqslant t''$) are:

(i) for the alloys with $x \leqslant 6$ and $y \leqslant 1$ the 'in-field' and the spontaneous magnetization follow the temperature variation predicted by equation (24) (equation (30)) with $H \neq 0$ and $H = 0$ in the interval $t^{**} \leqslant t \leqslant t^{***}$ ($t' \leqslant t \leqslant t''$), whereas the observed temperature dependence of $M(T, 0)$ and $M(T, H)$ for the alloys with $x = 8$ and 10 over the range $t^{\dagger} \leqslant t \leqslant t^{\dagger\dagger}$ is more accurately reproduced by equation (25) than by equation (24) (see figures 4–7), and

(ii) the coefficients A and A' of the T^2- and $T^{4/3}$-terms in equations (24) and (30) decrease with increasing external field strength for a given composition and with increasing Co concentration for a given H_{ext}-value including zero (figure 8).

The dependence of the coefficients A and A' on the effective field, defined as $H_{eff} = H - 4\pi N\langle M\rangle$ where N is the demagnetizing factor and $\langle M\rangle$ is the *average* value of the magnetization over the temperature range of the fit based on either equation (24) or equation (30), for different compositions is clearly brought out in figure 14. Though a brief account of the above observations (i) and (ii) has been given elsewhere [44], these results have been put in a proper perspective and discussed at length in this paper.

In view of equation (23), the finding that the expressions (24) and (25) reproduce

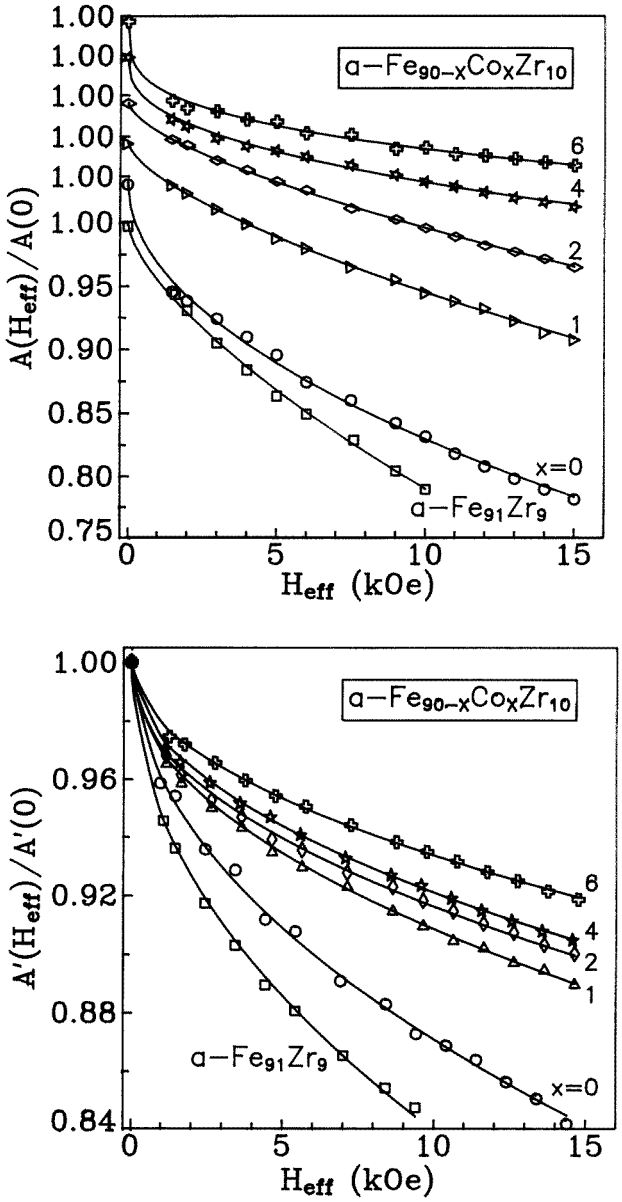

Figure 14. Variations of the coefficients $A(H_{eff})$ and $A'(H_{eff})$ with H_{eff} for different Co concentrations and for a-$Fe_{91}Zr_9$.

closely the observed variation of $M(T, 0)$ and $M(T, H)$ with temperature for the alloys with $0 \leqslant x \leqslant 6$, $y \leqslant 1$ and $x = 8$, 10, respectively (observation (i), above), implies that the T^4-term in equation (23) makes a significant contribution to $M(T, 0)$ and $M(T, H)$ only for the first set of alloys—presumably due to a sizable value of the Stoner enhancement factor S. To verify this, values of $\chi(0, 0)$ and $M(0, 0)$ (and hence μ_0) for each alloy are computed respectively from the slope and intercept (on the ordinate) of the (M^2 versus H/M) plot at $T = 5$ K, constructed from the $M(T, H)$ data taken at 5 K (figure 10). From the values

of these quantities so obtained and listed in table 4, one can, in principle, calculate various band and exchange parameters using equations (6)–(11) provided that the actual shape of the density of states (DOS) curve for each composition is known. In the absence of any such information, the values of S displayed in table 4 are deduced from equation (6) by making use of the values of $\chi(0,0)$ determined here and those of $N(E_F)$ estimated from the coefficient $\gamma_E = (\pi^2 k_B^2/3)N(E_F)$ of the electronic specific heat reported in the literature [45, 46] for the glassy alloys in question, after making corrections [46] for the electron–phonon enhancement. Note that the values of $N(E_F)$ for Co concentrations other than $x = 0$, 4 and 10 are the interpolated values obtained by passing a cubic spline through the data points in the $N(E_F)$ versus x plot [45] over the concentration range $0 \leqslant x \leqslant 30$. The data presented in table 4 clearly demonstrate that (a) S does indeed possess large values for $x \lesssim 6$ and decreases rapidly with increasing x and (b) the Stoner parameter I and hence also the exchange splitting of the bands $\Delta E = IM(0,0)/N\mu_B$ increase with x while $N(E_F)$ decreases with x such that the Stoner criterion for ferromagnetism, i.e., $IN(E_F) > 1$, is satisfied for all of the compositions. A direct consequence of the increase in ΔE with x is that the excitation of single particles and—more so—the formation of correlated particle–hole pairs (local spin-density fluctuations) becomes increasingly difficult as x is increased. This leads to a progressive suppression of spin fluctuations with Co substitution (figure 8). In view of the above arguments and the fact that both the Stoner–Wohlfarth [12, 13] and spin-fluctuation [11] models predict an extremely large value for the high-field susceptibility at low temperatures particularly for weak itinerant ferromagnets, the observed Co concentration dependence of χ_{hf} (see the inset of figure 11) is basically a manifestation of the progressive suppression of the weak itinerant nature of the ferromagnetism (i.e., a progressive *tendency* towards strong itinerant ferromagnetism) in the systems investigated here with increasing x.

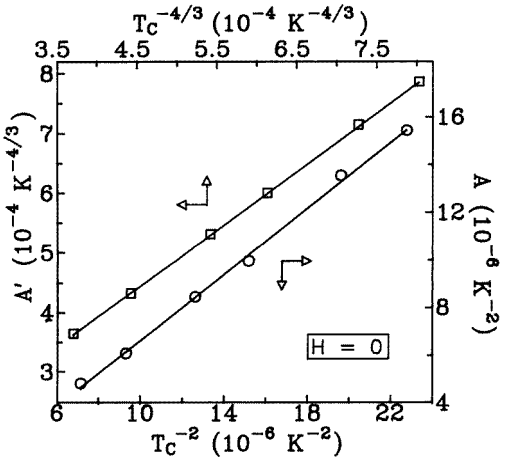

Figure 15. $A(H_{eff} = 0)$ versus T_C^{-2} and $A'(H_{eff} = 0)$ versus $T_C^{-4/3}$ plots.

Considering the well-known fact that by holding the weak temperature dependence of the thermal density of states (the one-electron density of states multiplied by the Fermi function) solely responsible for the T^2-decrease of $M(T,0)$, the Stoner model grossly overestimates T_C, $T_C^S \gg T_0$ in equation (23) and hence $T_0 \simeq T_C$. Alternatively, if local spin-density fluctuations dominantly contribute to the thermal demagnetization of $M(T,0)$ over the intermediate-temperature range and for temperatures close to T_C, one expects $T_C \approx T_0$

Table 5. A comparison of the spin-fluctuation temperatures with the Curie temperature.

Concentration y/x	T_C (K)	T_C^* (K)	T_C^*/T_C	T_1 (K)	T_1/T_C
$y = 1$	209.66(5)	180(1)	0.86(1)	213(1)	1.016(5)
$x = y = 0$	225.00(5)	193(3)	0.86(1)	229(2)	1.018(9)
$x = 1$	256.66(5)	227(1)	0.88(1)	261(2)	1.017(9)
$x = 2$	281.60(5)	244(3)	0.87(1)	286(3)	1.016(10)
$x = 4$	327.95(5)	286(2)	0.87(1)	334(3)	1.018(10)
$x = 6$	374.75(5)	323(6)	0.86(2)	380(3)	1.014(9)
$x = 8$	419.50(10)	[362(5)][a]	[0.86(1)][a]		
$x = 10$	462.50(10)	[398(6)][a]	[0.86(1)][a]		

[a] Values obtained from the estimates of $A''(0)$ given in table 2.

and $T_1 \simeq T_C$ from equations (23) and (28), respectively. That this is indeed the case is confirmed by the values of T_C^* and T_1 calculated from the relations $T_C^* = [A(0)]^{-1/2}$ ($T_C^* = [2A''(0)]^{-1/2}$) and $T_1 = [A'(0)]^{-3/4}$ using the values of $A(0)$ ($A''(0)$) and $A'(0)$ determined here, for the alloys with $x \leqslant 6$ ($x = 8$ and 10) and $y = 0$, 1, in that $T_C^*/T_C = 0.86(1)$ and $T_1/T_C = 1.02(1)$ regardless of the alloy composition (table 5). Since these ratios are constant over the composition range investigated, it is not surprising that the coefficients $A(0)$ and $A'(0)$ scale with T_C^{-2} and $T_C^{-4/3}$ (figure 15) in accordance with the predictions of the SF model. The results $A(0) \propto T_C^{-2}$ and $A'(0) \propto T_C^{-4/3}$ together with the finding that T_C increases with x (figure 12) offer a simple explanation for the reduction of $A(0)$ and $A'(0)$ with increasing x or, equivalently, for the suppression of the spin fluctuations with Co substitution. When the Co concentration is increased beyond $x = 6$, the contribution to $M(T, 0)$ arising from spin fluctuations diminishes at a rapid rate, with the result that it is reduced to an insignificant level for compositions in the vicinity of $x = 90$. In other words, the reduction of $M(T, 0)$ with T over the intermediate-temperature range for a-$Co_{90}Zr_{10}$ is mainly due to Stoner single-particle excitations. Thus, a-$Co_{90}Zr_{10}$ represents the extreme situation in which the particle–hole pair excitations are *weakly* correlated and $T_C^S \simeq T_C$.

A rapid reduction in the magnitude of $A(H_{eff})$ or $A'(H_{eff})$ with increasing H_{eff} (figure 14) is a clear indication of the suppression of spin fluctuations by the field. The effect of increasing magnetic field in the itinerant-electron picture is to increase the splitting between spin-up and spin-down sub-bands and hence, in analogy with the influence of the increase in ΔE caused by Co substitution on spin fluctuations discussed above, field, like x, strongly suppresses local spin-density fluctuations. It is seen from figure 14 that the rate at which the coefficient A or A' decreases with H slows down considerably as x increases. In view of the observation that, even in the absence of H, progressive replacement of Fe by Co leads to a strong suppression of SF, the coefficients A and A' are far less *sensitive* to H for higher Co concentrations than for lower values of x, because at higher Co concentrations, SF are already suppressed to a large extent even at $H = 0$ and the effect of H is reduced to a relatively insignificant level. An extreme situation arises when the Co concentration

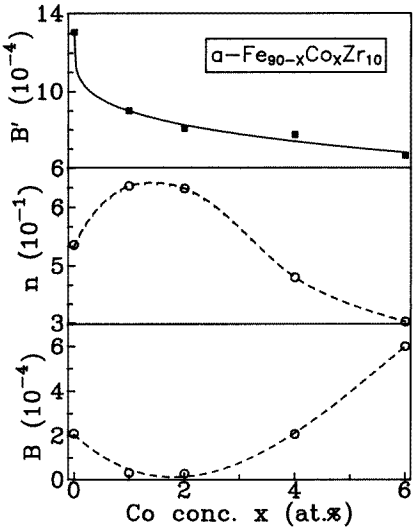

Figure 16. Fitting parameters for the LS fits to the $A(H_{eff})$ and $A'(H_{eff})$ data based on equation (35) of the text.

approaches $x = 90$ in that spin fluctuations are completely suppressed even in the absence of H and no further suppression is possible with H_{ext}. This inference conforms very well with our earlier observation [9] that $M(T, 0)$ and $M(T, H)$ data even for fields as high as 15 kOe coincide with one another at all temperatures below 300 K in the case of a-$Co_{90}Zr_{10}$. Another important finding that merits attention is that the empirical relation

$$\mathcal{A}(H_{eff}) = \mathcal{A}(0)[1 - \beta H_{eff}^{\eta}] \tag{35}$$

where $\mathcal{A}$, β and η stand for A or A', B or B' and the exponent n or n', respectively, closely reproduces the variation of A or A' with H_{eff} observed for the compositions $x \leqslant 6$ and $y = 0$, 1 with the choice of the parameters B, n, B' given in figure 16 and $n' = 0.50(2)$ as is evident from figure 14 in which the theoretical variation predicted by equation (35) is depicted by continuous curves. The $\sqrt{H_{eff}}$ power-law dependence of A on H_{eff} is highlighted by the $A'(H_{eff})/A'(0)$ versus $H_{eff}^{1/2}$ plot shown in figure 17. While the exponent n' is *independent* of composition over the range $0 \leqslant x \leqslant 6$, $0 \leqslant y \leqslant 1$, the slope B' decreases with increasing x in accordance with the empirical relation $B'(x) = B'(0)[1-\mu x^{\nu}]$ as is seen from figure 16 in which the continuous curve represents the composition dependence predicted by this relation for the parameter values $\mu = 4.15(5) \times 10^{-4}$ and $\nu = 0.25(2)$ using the observed value $B' = 1.30(2) \times 10^{-3}$.

The theoretical attempts [40, 47] made so far to quantify the suppression of spin fluctuations by external magnetic fields within the framework of the spin-fluctuation model cannot be regarded as satisfactory because a *large number* of adjustable parameters and the *unrealistic* electron-gas model have been used to achieve quantitative agreement with the experimental $M(T, H)$ data. Moreover, the same $M(T, H)$ data for Sc_3In have found qualitative explanation in terms of a band model [48] which does not take into account the local spin-density fluctuations and differs from the Stoner model in that, in addition to the Stoner exchange interaction parameter I, it has another interaction parameter (a nearest-neighbour ferromagnetic exchange interaction J) that gives rise to a temperature- and magnetization-dependent band narrowing. However, even this qualitative agreement

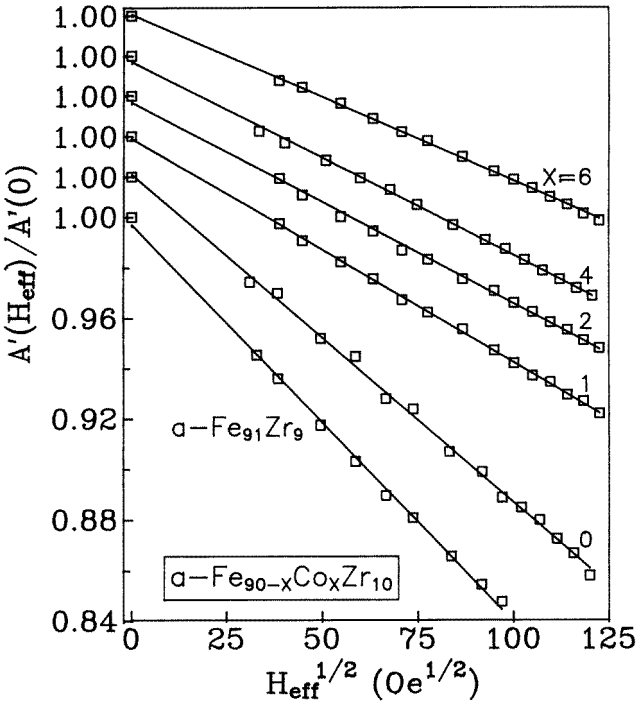

Figure 17. $A'(H_{eff})/A'(0)$ versus $H_{eff}^{1/2}$ plots for different compositions.

between the experimental data and the variation predicted by the latter theoretical treatment [48] cannot be relied upon because this model fails to reproduce the experimental variations, e.g., the $T^{4/3}$-dependence of $M(T, 0)$ and the $T^{5/3}$-dependence of the resistivity over certain temperature ranges, which the spin-fluctuation model successfully does. Another point that deserves a mention at this stage is that while attempting a quantitative comparison between theory and experiment [40, 47] due consideration has not been given to the observation that different types of excitation are primarily responsible for the decay of the magnetization in different temperature ranges. The limitation of the SF model as regards making specific predictions about the effect of field on SF stems from the fact that SF do not explicitly depend on H_{ext} but, by virtue of their dependence on M, indirectly couple to H_{ext} via magnetization. However, for temperatures close to T_C, great simplification results from the fact that the Bose function $n(\omega) \simeq k_B T/\hbar\omega$ and $\chi_{\parallel}^{-1} \simeq \chi_{\perp}^{-1}$, and the 'in-field' magnetization can be put into the form [49]

$$\left[\frac{M(T,H)}{M(0,0)}\right]^2 = 1 - \left(\frac{T}{T_C}\right)^{4/3}\left[1 - \frac{\pi}{2q_c}\left(\frac{g\mu_B}{D_{SF}}\right)^{1/2}\sqrt{H}\right] \tag{36}$$

where q_c is the temperature-dependent cut-off wave vector [11]. Thus the SF model correctly predicts the $\sqrt{H}$-dependence of the coefficient A', and in the light of equation (30), equation (36) has the same form as equation (35) with $B' = (\pi/2q_c)(g\mu_B/D_{SF})^{1/2}$. Since the value of q_c depends on the band-structure details, which are lacking at present, we assume that $q_c \simeq 1$ Å^{-1} (*irrespective* of composition) and insert this value plus those determined here (tables 1 and 2) for the spin-wave stiffness D as crude estimates for the stiffness coefficient for spin fluctuations for different compositions and $g = 2.07(2)$,

previously deduced from FMR measurements [16], in the above expression, with the result that $B' = 9.6 \times 10^{-4}$ and 8.1×10^{-4} for the alloys with $x = 0$ and 6 as against the observed values of 13.0×10^{-4} and 6.6×10^{-4}. From this comparison, one may be tempted to conclude that the SF model predicts a much slower decrease of the coefficient B' with x than the observed one. But when it is realized that both the quantities c_v (the coefficient of the gradient term in the Ginzburg–Landau expansion) and γ', appearing in the expression [11] $q_c \simeq (k_B T/\hbar\gamma_v' c_v)^{1/3}$, decrease rapidly with x because these alloys become more and more homogeneous magnetically and $N(E_F)$ falls steeply as the Co concentration is increased, a much closer agreement between the theoretical and experimental variation of B' with x is expected. For a quantitative comparison between theory and experiment, values of c_v and γ_v' for different compositions are needed. Such data are not available at present. Moreover, a theory, based on the SF model, which offers a quantitative explanation for the field dependence of the coefficient A observed in the intermediate-temperature range is called for. Note that none of the observations made in this section can be explained by the *homogeneous* transverse spin-freezing model [25], which is based on the Heisenberg model, since it predicts spin waves as the only low-lying magnetic excitations and thereby makes *no provision* for spin fluctuations.

Finally, certain issues that include the application of the spin-fluctuation (SF) model to the type of spin system under consideration need to be addressed. From a purist point of view, this model is strictly valid for *nearly* ferromagnetic metals or ferromagnetic metals with *unsaturated* moments only. Therefore, a direct application of the SF model to a concentrated system with 90 at.% or more 3d-transition-metal content would seem to be far fetched unless due consideration is given to the fact that the ferromagnetic ground state in a-$Fe_{100-p}Zr_p$ alloys becomes *unstable* [23, 24] when $p = p_c \simeq 7$ at.% and the alloys with y = 0, 1 and x = 0, 1, in particular, have a composition close to p_c, for which the ferromagnetic instability occurs. Another relevant point to note is that the generalizations of the SF model [50–52] that, besides the *'on-site'* exchange interaction I, include *inter-atomic* exchange interactions have recently been quite successful in *quantitatively* predicting the finite-temperature magnetic properties of the elemental ferromagnets Fe, Co and Ni. With these modifications, the SF model is now applicable to spin systems with reasonably large magnetic moments and Curie temperatures as well. It is in this context that the K (infinite 3D FM matrix plus finite FM clusters) model [2] (according to which weak itinerant-electron ferromagnetism and Invar behaviour are *inherent* properties of the infinite 3D FM matrix whereas the thermomagnetic and thermoremanent effects are associated with the spin-glass behaviour of the finite FM clusters once they are frozen in random orientations below a certain temperature T_{RE}) represents a generalization of the SF model that includes, besides the inter-atomic exchange interactions, other complexities present in the spin systems under consideration.

5. Conclusions

On the basis of an elaborate analysis of the magnetization data taken over a wide range of temperatures and external magnetic fields for amorphous $Fe_{90-x}Co_xZr_{10}$ (x = 0, 1, 2, 4, 6, 8, 10) and $Fe_{90+y}Zr_{10-y}$ (y = 0, 1) alloys and a detailed discussion of the results, the following conclusions can be drawn.

(i) The magnetization at 5 K does not saturate even for fields as high as 70 kOe for any of the alloys studied—the more so for those with $x \lesssim 6$ and $y \leqslant 1$. The high-field differential susceptibility, $\chi_{hf}(0)$, is extremely large for the alloys with x = 0, 1 and $y = 0$, 1

and decreases rapidly with increasing x for $x \lesssim 4$, and so it possesses values typical of the crystalline counterparts for $x > 6$. The large value of $\chi_{hf}(0)$ strongly indicates the presence of spin canting and weak itinerant ferromagnetism in the alloys with $x \lesssim 6$ and $y \leqslant 1$.

(ii) While spin-wave excitations are mainly responsible for thermal demagnetization of the spontaneous as well as 'in-field' magnetization at low temperatures ($T \lesssim 0.4T_C$), enhanced fluctuations in the local magnetization give the dominant contribution to $M(T, 0)$ over a wide range of intermediate temperatures ($0.45T_C \lesssim T \lesssim 0.75T_C$) and for temperatures close to T_C ($0.7T_C \lesssim T \lesssim 0.95T_C$) for all of the alloys. In the a-$Co_{90}Zr_{10}$ alloy, the dominant spin-wave contribution to both $M(T, 0)$ and $M(T, H)$ at low temperatures ($T \lesssim 0.1T_C$) is followed by an overwhelming contribution from Stoner single-particle excitations at higher temperatures, implying thereby that the particle–hole pair excitations are very *weakly correlated* in this case.

(iii) The spin-wave stiffness coefficient D is *independent* of the external field for all of the compositions while the D/T_C ratio possesses a value $\simeq 0.14$ for the alloys with $y = 0, 1$ and $x \leqslant 6$ which is *characteristic* of amorphous ferromagnets with *competing* interactions.

(iv) The observed temperature renormalization of D agrees well with the temperature variation predicted by the itinerant-electron model and indicates that the magnon–spin-fluctuation interactions are more important in these systems than the magnon–magnon interactions.

(v) For the compositions $x \lesssim 6$ and $y = 0, 1$, the value of D directly measured in inelastic neutron scattering (INS) experiments, D_N, is expected to greatly exceed that deduced from the magnetic measurements, D_M. This is so because, in these alloys, 'diffusons' (non-propagating longitudinal spin fluctuations) contribute to the $T^{3/2}$-decrease of the magnetization as significantly as the propagating transverse spin fluctuations (spin waves) do, but they (the diffusons) show up as an elastic peak in the INS spectra.

(vi) The infinite three-dimensional ferromagnetic (FM) matrix plus finite FM clusters model as well as the spin-fluctuation model offer a straightforward explanation not only for the absence of spin-wave peaks in the INS spectra taken for the wave-vector-transfer range $0.05\ \text{Å}^{-1} \leqslant q \leqslant 0.12\ \text{Å}^{-1}$ but also for the composition dependence of $D(0)$, T_C, $M(0, 0)$ and $\chi_{hf}(0)$.

(vii) In accordance with the predictions of the spin-fluctuation model, spin fluctuations get strongly suppressed by Co substitution and external magnetic fields. This model provides a consistent theoretical basis for the observed temperature dependence of the spontaneous and 'in-field' magnetization over the entire temperature range $0 \lesssim T \lesssim T_C$.

(viii) The Stoner criterion $IN(E_F) > 1$ for the occurrence of ferromagnetism is satisfied. All of the alloys studied in this work are *weak* itinerant ferromagnets.

(ix) Contrary to the claim [53] made recently that the *homogeneous* transverse spin-freezing model [25] provides an adequate description of magnetism in a-$Fe_{90\pm y}Zr_{10\mp y}$ alloys, most of our observations do not find any explanation in terms of this model.

Acknowledgments

The authors are grateful to Professor H Kronmüller for permitting the use of the SQUID magnetometer and to Dr M Seeger for his help in performing the SQUID measurements.

References

[1] Kaul S N 1983 *Phys. Rev.* B **27** 6923
[2] Kaul S N 1991 *J. Phys.: Condens. Matter* **3** 4027

[3] Kaul S N, Siruguri V and Chandra G 1992 *Phys. Rev.* B **45** 12 343
[4] Fish G E and Rhyne J J 1987 *J. Appl. Phys.* **61** 454
Rhyne J J, Erwin R W, Fernandez-Baca J A and Fish G E 1988 *J. Appl. Phys.* **63** 4080
[5] Fernandez-Baca J J, Lynn J W, Rhyne J J and Fish G E 1988 *J. Appl. Phys.* **63** 3749
[6] Yu S C, Lynn J W and Fish G E 1993 *Japan. J. Appl. Phys.* **32** 67
[7] Shirakawa K, Ohnuma S, Nose M and Masumoto T 1980 *IEEE Trans. Magn.* **16** 910
Ohnuma S, Shirakawa K, Nose M and Masumoto T 1980 *IEEE Trans. Magn.* **16** 1129
[8] Tange H, Inoue K and Shirakawa K 1986 *J. Magn. Magn. Mater.* **54–57** 303
Tange H, Kobayashi S, Kawabuchi S, Kamimori T and Goto M 1992 *J. Magn. Magn. Mater.* **109** 169
[9] Kaul S N and Babu P D 1992 *J. Phys.: Condens. Matter* **4** 6429
[10] Babu P D, Kaul S N, Fernández Barquin L and Gómez Sal J C 1995 *J. Magn. Magn. Mater.* **140–144** 295
[11] Lonzarich G G and Taillefer L 1985 *J. Phys. C: Solid State Phys.* **18** 4339
Lonzarich G G 1986 *J. Magn. Magn. Mater.* **54–57** 612
[12] Mathon J and Wohlfarth E P 1968 *Proc. R. Soc.* A **302** 409
Edwards D M and Wohlfarth E P 1968 *Proc. R. Soc.* A **303** 127
[13] De Chatel P F and De Boer F R 1970 *Physica* **48** 331
Wohlfarth E P and De Chatel P F 1970 *Physica* **48** 477
[14] Continentino M A and Rivier N 1979 *J. Phys. F: Met. Phys.* **9** L145
Rivier N and Continentino M A 1980 *J. Magn. Magn. Mater.* **15–18** 1419
[15] Kaul S N 1981 *Phys. Rev.* B **23** 1205
[16] Kaul S N and Babu P D 1992 *Phys. Rev.* B **45** 295
[17] Babu P D and Kaul S N 1997 *J. Phys.: Condens. Matter* **9** 7189
[18] Kaul S N and Babu P D 1994 *Phys. Rev.* B **50** 9308
[19] Hiroyoshi H and Fukamichi K 1982 *J. Appl. Phys.* **53** 2226
[20] Deppe P, Fukamichi K, Li F S, Rosenberg M and Sostarich M 1984 *IEEE Trans. Magn.* **20** 1367
[21] Kiss L F, Kemény T, Vincze I and Gránásy L 1994 *J. Magn. Magn. Mater.* **135** 161
[22] Kaul S N 1984 *IEEE Trans. Magn.* **20** 1290
Kaul S N 1985 *J. Magn. Magn. Mater.* **53** 5
[23] Beck W and Kronmüller H 1985 *Phys. Status Solidi* **132** 449
Ryan D H, Coey J M D, Batalla E, Altounian Z and Ström-Olsen J O 1987 *Phys. Rev.* B **35** 8630
[24] Read R A, Moyo T and Hallam G C 1986 *J. Magn. Magn. Mater.* **54–57** 309
[25] Ryan D H, Ström-Olsen J O, Provencher R and Townsend M 1988 *J. Appl. Phys.* **64** 5787
[26] Gabay M and Toulouse G 1981 *Phys. Rev. Lett.* **47** 201
[27] Senousii S and Elkhatouri D 1986 *J. Magn. Magn. Mater.* **54–57** 153
[28] Campbell I A and Senousii S 1992 *Phil. Mag.* B **65** 1267
[29] Kaul S N 1995 *Met., Mater. Process.* **7** 29
[30] Krishnan R, Rao K V and Liebermann H H 1984 *J. Appl. Phys.* **55** 1823
[31] Siruguri V and Kaul S N 1996 *J. Phys.: Condens. Matter* **8** 4545
[32] Kaul S N 1983 *Phys. Rev.* B **27** 5761
[33] Dey S, Gorres U, Nielsen H J V, Rosenberg M and Sostarich M 1980 *J. Physique Coll.* **41** C8 678
Dey S, Deppe P, Rosenberg M, Luborsky F E and Walter J L 1981 *J. Appl. Phys.* **52** 1805
[34] Soumura T, Takeda K, Wakano T, Terasawa K and Maeda T 1986 *J. Magn. Magn. Mater.* **58** 202
[35] Kaul S N and Mohan Babu T V S M 1989 *J. Phys.: Condens. Matter* **1** 8509
[36] Birgeneau R J, Tarvin J A, Shirane G, Gyorgy E M, Sherwood R C, Chen H S and Chien C L 1978 *Phys. Rev.* B **18** 2192
[37] Hilscher G, Haferl R, Kirchmayr H, Müller M and Güntherodt H J 1981 *J. Phys. F: Met. Phys.* **11** 2429
[38] Katsuki A and Wohlfarth E P 1966 *Proc. R. Soc.* A **295** 182
Katsuki A 1967 *Br. J. Appl. Phys.* **18** 199
Wohlfarth E P 1966 *Quantum Theory of Atoms, Molecules, and the Solid State* ed P Löwdin (New York: Academic) p 485
[39] Kaul S N 1988 *J. Phys. F: Met. Phys.* **18** 2089
[40] Moriya T 1984 *J. Magn. Magn. Mater.* **31–34** 10
Moriya T 1979 *J. Magn. Magn. Mater.* **14** 1
Moriya T 1985 *Spin Fluctuations in Itinerant Electron Magnetism* (Berlin: Springer)
[41] Singh A and Tešanović Z 1989 *Phys. Rev.* B **39** 7284
[42] Singh V A and Roth L M 1978 *J. Appl. Phys.* **49** 1642
Kaneyoshi T 1978 *J. Phys. Soc. Japan* **45** 1835
[43] Iskhakov R S 1977 *Fiz. Tverd. Tela* **19** 3 (Engl. Transl. 1977 *Sov. Phys.–Solid State* **19** 1)

[44] Babu P D and Kaul S N 1997 *J. Phys.: Condens. Matter* **9** 3625
[45] Rosenberg M, Hardebusch U, Schöne-Warnefeld A, Wernhardt R and Fukamichi K 1988 *J. Phys. F: Met. Phys.* **18** 2259
[46] Kanemaki S, Takehira O, Fukamichi K and Mizutani U 1989 *J. Phys.: Condens. Matter* **1** 5903
[47] Takeuchi J and Masuda Y 1979 *J. Phys. Soc. Japan.* **46** 468
[48] Hirsch J E 1991 *Phys. Rev.* B **44** 675
[49] Kaul S N, unpublished results
[50] Mohn P and Wohlfarth E P 1987 *J. Phys. F: Met. Phys.* **17** 2421
[51] Uhl M and Kübler J 1996 *Phys. Rev. Lett.* **77** 334
Uhl M and Kübler J 1997 *Physica* B **237–238** 496
[52] Rosengaard N M and Johansson B 1997 *Phys. Rev.* B **55** 14 975
[53] Ren H and Ryan D H 1995 *Phys. Rev.* B **51** 15 885